

Review

# Assessment of the Diagnostic Performance and Clinical Impact of AI in Hepatic Steatosis: Systematic Review and Meta-Analysis

Jiamei Song\*, MM; Dan Liu\*, MS; Jitong Li, MM; Haoru Cong, MM; Ruixue Deng, MM; Yihan Lu, MBBS; Jiayi Sun, MBBS; Jingzhou Zhang, MD

College of Traditional Chinese Medicine, Changchun University of Chinese Medicine, Changchun, Jilin, China

\*these authors contributed equally

**Corresponding Author:**

Jingzhou Zhang, MD

College of Traditional Chinese Medicine

Changchun University of Chinese Medicine

No 1035, Boshuo Road Jingyue National High-Tech Industrial Development Zone Changchun City

Changchun, Jilin 130117

China

Phone: 86 13756864698

Email: [zjz362@126.com](mailto:zjz362@126.com)

## Abstract

**Background:** The global rise of metabolic associated fatty liver disease reflects the urgent need for accurate, noninvasive diagnostic approaches. The invasive nature of liver biopsy and the limited sensitivity of ultrasound in detecting early steatosis highlight a critical diagnostic gap. Artificial intelligence (AI) has emerged as a transformative tool, enabling the automated detection and grading of hepatic steatosis (HS) from medical imaging data.

**Objective:** This review aims to quantitatively evaluate the diagnostic performance of AI models for HS, explore sources of interstudy heterogeneity, and provide an appraisal of their clinical applicability, translational potential, and the major barriers impeding widespread implementation.

**Methods:** PubMed, Cochrane Library, Embase, Web of Science, and IEEE Xplore databases were searched until September 24, 2025. Studies using AI for HS diagnosis, meeting predefined PIRT (Patient Selection, Index Test, Reference Standard, Flow and Timing) framework and providing extractable data were included. Diagnostic performance indicators, including sensitivity, specificity, and the area under the summary receiver operating characteristic curve (AUC), were extracted and quantitatively synthesized. Meta-analyses were conducted using a bivariate random effects model. The methodological quality and risk of bias were evaluated using the QUADAS-2 (Quality Assessment of Diagnostic Accuracy Studies 2) tool. Heterogeneity was assessed through the  $I^2$  statistic, bivariate box plots, 95% PIs, and threshold effect analysis. Clinical applicability was examined using the Fagan nomogram and likelihood ratio tests.

**Results:** A total of 36 eligible studies were identified, of which 33 (comprising 36 cohorts) were included in the subgroup analyses. Results demonstrated excellent diagnostic accuracy of AI models, with a summary sensitivity of 0.95 (95% CI 0.93-0.96), specificity of 0.93 (95% CI 0.91-0.94), and an AUC of 0.98 (95% CI 0.96-0.99). Clinical applicability analysis (positive likelihood ratio  $>10$ ; negative likelihood ratio  $<0.1$ ) supported AI's strong potential for both confirming and excluding HS. However, substantial heterogeneity was observed across studies ( $I^2 >75\%$ ). According to QUADAS-2, a high risk of bias, particularly in the Patient Selection domain (44.4%), may have contributed to the overestimation of real-world performance. Subgroup analyses showed that deep learning models significantly outperformed traditional machine learning approaches (AUC: 0.98 vs 0.94). Models using ultrasound or histopathology references, retrospective designs, transfer learning, and public datasets achieved the highest accuracy (AUC 0.98-0.99) but contributed to interstudy heterogeneity.

**Conclusions:** AI demonstrates remarkable potential for noninvasive screening and assessment of HS, especially in primary care. Nonetheless, clinical translation remains limited by performance variability, retrospective designs, lack of external validation, practical barriers such as data privacy and workflow integration. Future studies should prioritize prospective multicenter trials and standardized external validation to bridge the gap between current evidence and clinical application. The

key innovation of this review lies in establishing a unified, modality-agnostic analytical framework that integrates evidence beyond single-modality evaluations.

**Trial Registration:** PROSPERO CRD420251046862; <https://www.crd.york.ac.uk/PROSPERO/view/CRD420251046862>

*J Med Internet Res* 2026;28:e78310; doi: [10.2196/78310](https://doi.org/10.2196/78310)

**Keywords:** artificial intelligence; AI; diagnostic performance; hepatic steatosis; meta-analysis; clinical impact

## Introduction

Metabolic-associated fatty liver disease (MAFLD) has emerged as one of the most prevalent chronic liver diseases worldwide, with its pathophysiology intrinsically linked to metabolic syndrome. Affected individuals frequently exhibit concomitant metabolic abnormalities such as central obesity, type 2 diabetes mellitus, and insulin resistance. The disease spectrum of MAFLD represents a continuum ranging from simple hepatic steatosis (HS) to metabolic dysfunction-associated steatohepatitis (MASH), which may progress to hepatic fibrosis, cirrhosis, or hepatocellular carcinoma (HCC) [1]. Therefore, MAFLD is a significant and growing global public health threat [2].

In 2020, an international consensus panel proposed renaming “non-alcoholic fatty liver disease” to “MAFLD” to better reflect its metabolic foundation [3,4]. To ensure the present study focuses on the diagnostic performance of artificial intelligence (AI) for the core pathological feature of HS and to enhance its clinical generalizability, including to populations with mixed etiologies such as concomitant metabolic disorders and alcohol use, we adopted the broader term “MAFLD.” This terminology aligns more closely with real-world clinical practice and provides a consistent framework for AI model training and validation. Epidemiological data estimate the global prevalence of MAFLD at approximately 38%, with substantial regional variation, the highest burdens observed in Latin America, the Middle East, and North Africa [5]. The disease is also increasingly recognized among pediatric and adolescent populations, particularly in individuals with obesity, where prevalence rates have been reported to range from 7% to 14% or higher [6].

Nevertheless, the reported MAFLD prevalence varies markedly across studies, from 5% to 46% [7], reflecting considerable heterogeneity. First, diagnostic methodologies differ. Although liver biopsy remains the histopathological gold standard, its invasiveness limits clinical use, shifting reliance toward multimodal imaging. Noninvasive modalities such as ultrasound and computed tomography (CT) are widely used due to accessibility and low cost, but they lack precision in quantifying HS. Quantitative imaging techniques, including magnetic resonance imaging–proton density fat fraction (MRI-PDFF) [8], controlled attenuation parameter-based transient elastography, and noninvasive analysis [9], offer superior accuracy but are constrained by cost and limited availability. Clinical prediction models such as the Fatty Liver Index [10], Hepatic Steatosis Index [11], and Liver Fat Equation [12] enable noninvasive diagnosis through integration of anthropometric and

biochemical parameters. Nevertheless, they remain vulnerable to measurement variability and lack use for longitudinal monitoring. Second, the sensitivity of existing diagnostic modalities in detecting early-stage steatosis (hepatic fat content <5%) remains suboptimal. Conventional ultrasound, in particular, has a high false-negative rate when hepatic fat content falls below 20% [13], leading to underdiagnosis and misdiagnosis in subclinical populations.

Such diagnostic inaccuracies carry serious clinical implications. Patients erroneously classified as having “simple MASLD” but who also exhibit alcohol use disorder have been shown to experience mortality risks exceeding those of individuals with typical alcoholic liver disease [14]. As MAFLD incidence rises globally, associated cirrhosis and HCC cases are also increasing. Failure to achieve early and accurate diagnosis forfeits the therapeutic window during the reversible steatosis stage, allowing progression to MASH and fibrosis. Notably, MAFLD-related HCC may arise in noncirrhotic livers [15], challenging conventional surveillance strategies that primarily target cirrhotic patients. Moreover, MAFLD is an established independent risk factor for cardiovascular disease [16]. This elevated cardiovascular risk persists throughout the disease course and remains heightened even following liver transplantation [17], underscoring the necessity of lifelong risk management.

Recent advances in AI have revolutionized medical image analysis, and hepatology has been no exception. AI-based approaches have demonstrated strong diagnostic performance across multiple hepatic pathologies. For instance, Meng et al [18] developed a VGGNet-based multistage fibrosis classifier, achieving high accuracy across 3 fibrosis grades. Wang et al [19] introduced the Explainable Diagnosis Recommender intelligent diagnostic system, which uses deep learning (DL) to automatically detect hepatic echinococcosis and cysts from CT scans. Xiao et al [20] proposed a ResNet-101-based multimodal model that classified 6 hepatobiliary diseases using slit-lamp and fundus images, outperforming clinicians of varying experience levels. Calderaro et al [21] used a DL model to reclassify combined hepatocellular-cholangiocarcinoma into pure HCC or intrahepatic cholangiocarcinoma with high sensitivity and specificity, yielding predictions consistent with clinical and molecular profiles. Specifically for HS assessment, Yang et al [22] developed a 2-stage DL model that classified four steatosis grades with an overall accuracy of 76.3% and an area under the summary receiver operating characteristic (SROC) curve (AUC) of 0.88, surpassing traditional clinical indices. Similarly, Wang et al [23] employed DL to quantify hepatic fat content by inferring proton density fat fraction (PDFF) from routine T1-weighted magnetic

resonance imaging (MRI) images, surpassing the performance of the conventional 2-point Dixon fat-fraction model.

Despite these promising developments, the application of AI in the diagnosis and grading of MAFLD or HS remains at an early stage [24]. Existing systematic reviews have primarily assessed AI performance within individual imaging modalities. A critical gap remains: a comprehensive evaluation of AI's overall diagnostic efficacy across diverse imaging platforms and a systematic analysis of the key technical and methodological determinants of performance are still lacking.

Therefore, this study, for the first time, uses a bivariate mixed effects model [25] to systematically assess the overall diagnostic performance of AI in imaging-based detection of HS. The primary objectives are: (1) to quantitatively determine the aggregate diagnostic accuracy of AI models in identifying HS; (2) to comprehensively explore the sources of heterogeneity, with particular emphasis on the influence of factors such as algorithm type, reference standard, imaging modality, study design, and data accessibility; and (3) to evaluate the clinical applicability and translational potential of AI-based diagnostic systems, while identifying major barriers to their broad clinical adoption. Through these aims, the present study seeks to generate robust, high-level evidence that transcends the limitations of individual analytical approaches, thereby providing meaningful guidance for future research and clinical practice.

## Methods

### Research Design and Clinical Questions

This study protocol was registered with the PROSPERO International Prospective Register of Systematic Reviews (Registration: CRD420251046862). The research was conducted as per the PRISMA-DTA (Preferred Reporting Items for Systematic Reviews and Meta-Analyses-Diagnostic Test Accuracy) guidelines (Checklist 1) [26].

### Search Strategy

This systematic search was independently designed and conducted by two researchers as per the PRISMA-DTA (Checklist 1) [26]. PubMed, the Cochrane Library, Embase, Web of Science, and IEEE Xplore were retrieved until September 24, 2025. The search strategy was structured around three core concepts: (1) the disease (“HS,” “non-alcoholic fatty liver disease,” and “MAFLD”); (2) the technology (“AI,” “machine learning [ML],” “DL”); and (3) the diagnostic context (“diagnosis,” “detection”).

Keywords within each conceptual category were combined via the OR operator (eg, AI OR DL OR ML), whereas keywords across different categories were linked using the AND operator (eg, AI AND MAFLD AND diagnosis).

The authors of the identified studies were not contacted. Reference lists of all included studies were manually reviewed to identify any additional eligible publications. No restrictions on language or publication date were applied

at the database level to maximize search sensitivity. However, non-English records were excluded during subsequent screening. Gray literature, preprints, and unpublished studies were not systematically searched. This decision was made a priori to focus on peer-reviewed, full-text articles that had undergone editorial review, thereby ensuring baseline methodological quality and the availability of sufficient details for data extraction. The complete, reproducible search strings for all databases are provided in Table S1 in [Multimedia Appendix 1](#).

### Screening Process

Two independent reviewers initially screened all retrieved titles and abstracts. After removing duplicate records, studies were deemed eligible for inclusion if they met the following criteria:

- Study content: the research conformed to the predefined PIRT (Patient Selection, Index Test, Reference Standard, Flow and Timing) framework:
  - Patient Selection (P): patients undergoing abdominal imaging or pathological examination for HS assessment.
  - Index Test (I): AI models based on DL or ML, using input images derived from ultrasound, CT, MRI, or pathology.
  - Reference Standard (R): defined by the original studies, including MRI-PDFF, liver biopsy pathology, or expert-graded ultrasound. These reference standards reflect real-world diagnostic diversity and were recognized as potential sources of heterogeneity.
  - Target Condition (T): Diagnosis and grading of HS according to the thresholds and criteria adopted in the included studies, allowing cross-comparison of AI performance across varying diagnostic definitions.
- Data availability: studies had to provide diagnostic contingency data, true positives (TP), true negatives (TN), false positives (FP), and false negatives (FN), or sufficient information to derive diagnostic performance metrics, such as AUC with 95% CIs, sensitivity, specificity, accuracy, and predictive values.

Exclusion criteria were: (1) language: non-English publications; (2) study type: letters, conference abstracts, reviews, or academic papers lacking original data; (3) study subjects: animal or nonhuman research, bioinformatics-based analyses, and predictive modeling studies focused on indices, risks, or associations rather than diagnosis; and (4) data sufficiency: studies without key contingency data or insufficient information to calculate diagnostic performance metrics.

### Data Extraction

Two researchers independently extracted data based on the following domains: (1) study characteristics: first author, publication year, site of data collection, and duration of the study period; (2) study population: total sample size, and demographic characteristics (mean or median age); (3) methodological parameters: accessibility of clinical sample data, diagnostic reference standard, and validation strategy;

- (4) algorithmic architecture: type of algorithm, classifier employed, and application of transfer learning (TL); and
- (5) diagnostic efficacy: raw contingency table data, and aggregated diagnostic performance metrics.

## Diagnostic Performance Evaluation and Quality Assessment

Pooled estimates of sensitivity, specificity, and AUC, together with their 95% CIs, were presented using forest plots. Heterogeneity was quantified using the  $I^2$  statistic. The AUC was designated as the primary indicator for overall diagnostic accuracy, as it integrates performance across all thresholds and remains unaffected by any single cut-off point. A SROC curve was constructed following an assessment of the threshold effect using the Spearman correlation coefficient between the logit of sensitivity and the logit of (1-specificity). Heterogeneity and its implications were further visualized via 95% PIs and bivariate boxplots. Potential small-study effects were evaluated using the Deeks funnel plot asymmetry test. Additional diagnostic indicators, including the diagnostic odds ratio (DOR), positive likelihood ratio (LRP), and negative likelihood ratio (LRN), were calculated. Clinical applicability was further examined using a Fagan nomogram, while the distribution of likelihood ratios across studies was illustrated via scatterplots.

Two investigators assessed the risk of bias via the QUADAS-2 (Quality Assessment of Diagnostic Accuracy Studies 2) checklist (Checklist 2) in Rev-Man in terms of PIRT framework [27]. The QUADAS-2 tool, recommended by the Cochrane collaboration, was used to assess the methodological quality and risk of bias of included diagnostic accuracy studies.

## Quality Assurance and Dispute Resolution

All screening, data extraction, and quality assessment procedures were independently conducted by 2 reviewers. Any discrepancies were first resolved through discussion to reach a consensus. When consensus was not achieved, a third senior investigator adjudicated the disagreement to make the final determination. This multilevel process ensured that all extracted data represented unanimous agreement within the research team.

## Subgroup Analysis

The following independent meta-analyses were conducted:

1. AI type (ML versus DL): DL models were defined as those based on multilayer artificial neural networks, such as convolutional neural networks and recurrent neural networks (RNNs). This category included all studies that explicitly reported using DL or identified architectures such as VGG, ResNet, U-Net, DenseNet, or Inception. ML models referred to traditional algorithms that learn from data without relying primarily on deep neural architectures, including support vector machines (SVM), random forests, decision trees, and logistic regression. To

explore the potential influence of different algorithmic approaches on diagnostic performance.

2. Reference standards for steatosis grading (MRI-PDFF, liver histopathology, or ultrasound): to determine whether there was a performance gap between models based on noninvasive imaging and those based on the pathological “gold standard.”
3. Imaging modality (ultrasound, CT, or histopathology): to assess how differences in imaging principles, invasiveness, and the diagnostic information scale (macroscopic versus microscopic) affected model performance.
4. Application of TL: TL was used when a study explicitly reported the use of a model pretrained on a large-scale dataset (eg, ImageNet) as the initial framework for feature extraction or model fine-tuning. To evaluate whether this specific technique could improve model performance in small-sample medical datasets.
5. Study design (single-center versus multicenter): to assess the generalizability of models across different data distributions.
6. Study type (prospective vs retrospective): to explore the temporal relationship between data collection and model development and to evaluate the potential impact of selection bias on performance assessment.
7. Data accessibility: to evaluate the effect of study reproducibility and transparency on research outcomes.

## Data Analysis

Given the substantial heterogeneity observed among included studies with respect to patient populations, imaging devices, and AI algorithms, a bivariate mixed effects model was used to derive more accurate and reliable pooled estimates [25]. To ensure the robustness of the meta-analytic results, quantitative synthesis (eg, subgroup analysis) was performed only when at least 3 independent studies, defined as studies conducted by different authors, using distinct experimental protocols, or involving separate participant cohorts, were available. Multiple effect estimates from the same publication were included when they originated from distinct participant cohorts (eg, multicenter datasets or independent validation sets). When multiple model outputs were reported, only the best-performing model or that validated using an independent dataset was retained. Subgroup analyses were not conducted when fewer than three independent studies were available for a given subgroup. All statistical analyses and visualizations were performed via Stata MP 18 (StataCorp LLC). A 2-tailed  $P$  value  $<0.05$  denoted statistical significance.

## Results

### Included Study Description

As of September 24, 2025, 2536 articles were retrieved. After removing 864 duplicates, the titles and abstracts of the rest were screened as per the predefined eligibility criteria, resulting in the exclusion of 1596 articles. Specifically, 9 were non-English publications, 884 were of other types, 673 involved inappropriate study subjects, and 30 used

unsuitable research methods. The full texts of the remaining 76 articles were subsequently reviewed. Seventeen studies were excluded for incomplete data, 7 for being of other types, 7 for inappropriate methodologies, and 9 for being

inaccessible. Ultimately, 36 studies were included in the final analysis (Figure 1). The characteristics of the included studies are summarized in Table 1, and the results of the subgroup analyses are presented in Table 2.

**Figure 1.** PRISMA (Preferred Reporting Items for Systematic Reviews and Meta-Analyses—Search Extension) flowchart depicting the study selection process for the systematic review of artificial intelligence in diagnosing hepatic steatosis.

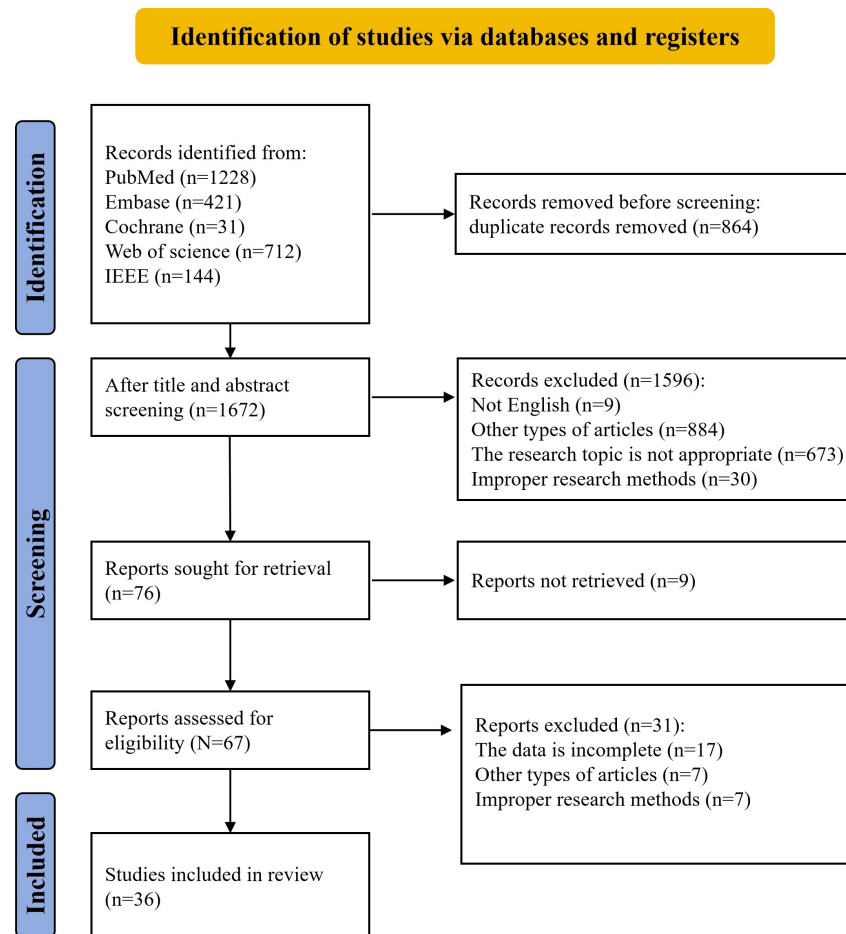


**Table 1.** Summary of study characteristics in the systematic review of artificial intelligence (AI)-assisted hepatic steatosis (HS) detection (N=36).

Number	Study	Device	DL <sup>a</sup> or ML <sup>b</sup>	TL <sup>c</sup>	Source of data	Data range	Sample size	Age, years	Open access data	Research type
1	Yang et al (2022) [28]	MRI <sup>d</sup>	DL	Yes	A hospital in Beijing	Jun-Jul 2020	50	• NR <sup>e</sup>	No	• Retrospective study
2	Acharya et al (2016) [29]	Ultrasound	DL	NR	The University of Malaya Medical Centre, Malaysia	NR	100	• NR	No	• Single-center study
3	Jeon et al (2023) [30]	Ultrasound	DL	NR	Seoul National University Hospital	Jul 2020-Jun 2021	173	• mean (SD): 51 (14)	No	• Prospective study
4	Neogi et al (2018) [31]	Ultrasound	DL	NR	Chittaranjan National Cancer Hospital	NR (a span of 6 months)	51	• range: 19-74 • NR	No	• Single-center study
5	Chen et al (2020) [32]	Ultrasound	DL	NR	Chang Gung Memorial Hospital in Taiwan	2017-2020	205	• mean (SD): 55 (11.6)	No	• Retrospective study
6	Dubois et al (2019) [33]	Ultrasound	DL	NR	Rennes University Hospital	Jun 2017-Aug 2018	53	• median (IQR): 61 (28-72)	No	• Prospective study
7	Shi et al (2019) [34]	Ultrasound	ML	NR	Shanghai Public Health Clinical Center	NR	60	• range: 19-69	No	• Single-center study

Number	Study	Device	DL <sup>a</sup> or ML <sup>b</sup>	TL <sup>c</sup>	Source of data	Data range	Sample size	Age, years	Open access data	Research type
8	Jesper et al (2020) [35]	Ultrasound	ML	NR	Erlangen University Hospital	Oct 2018-Sep 2019	27	• mean (SD): 50 (17)	No	• Prospective study • Single-center
9	McHenry et al (2020) [36]	MRI	DL	NR	Dallas County	2000-2002; 2007-2009	2139	• median: 44	No	• Prospective study • Single-center
10	Roy et al (2021) [37]	Pathology	DL	NR	Children's Hospital of Atlanta and Emory University	2014-2016	36	• mean (SD): 14.9 (2.59)	Yes	• Retrospective study
11	Sun et al (2020) [38]	Pathology	DL	Yes	Washington University School of Medicine Transplant Pathology Service	Apr 2015-Sep 2016	91	• NR	No	• Multicenter
12	Chou et al (2021) [39]	Ultrasound	DL	Yes	Taipei Medical University Hospital	2016-2018	2070	• NR	No	• Retrospective study
13	Constantinescu et al (2021) [40]	Ultrasound	DL	Yes	Outpatient clinic of a private healthcare network	NR	60	• range: 18-92	No	• Single-center
14	Pérez-Sanz et al (2021) [41]	Pathology	DL	NR	University Clinical Hospital Virgen de la Arrixaca-Biomedical Research Institute of Murcia	NR	20	• NR	No	• Retrospective study
15	Pickhardt et al (2020) [42]	CT	DL	NR	A single academic medical center	Feb 2010-Jan 2017	1204	• mean (SD): 45.2 (12.4)	No	• Single-center • Retrospective study

Number	Study	Device	DL <sup>a</sup> or ML <sup>b</sup>	TL <sup>c</sup>	Source of data	Data range	Sample size	Age, years	Open access data	Research type
16	Rhyou et al (2021) [43]	Ultrasound	DL	Yes	Samsung Medical Center and Byra Dataset	NR	• NR	Yes	• Single-center	
17	Destrempe et al (2022) [44]	Ultrasound	ML	NR	Center Hospitalier de l'Université de Montréal and McGill University Health Center	Oct 2014-Sep 2018	82	• mean (SD): 56 (12)	• Retrospective study	
18	Alshagathr et al (2023) [45]	Ultrasound	DL	Yes	University of Warsaw, Poland	NR	55	• range: 23-78	• Multicenter	
19	Podder et al (2023) [46]	Pathology	DL	Yes	Open Science Framework	NR	• NR	Yes	• Single-center	
20	Ibrahim et al (2023) [47]	Ultrasound	DL	Yes	Beijing You'an Hospital in Beijing, China, and the National Hepatology and Tropical Medicine Research Institute in Cairo, Egypt	NR	478	• mean (SD): 40.97 (10.61)	• Prospective study	
21	Yao et al (2023) [48]	Ultrasound	DL	Yes	Byra dataset and the Health Service Center in the Chenghua District of Chengdu	2020-2022	1320	• NR	• Single-center	
22	Byra et al (2018) [49]	Ultrasound	DL	Yes	Medical University of Warsaw, Poland	NR	55	• mean (SD): 40.1 (9.1)	• Multicenter	

Number	Study	Device	DL <sup>a</sup> or ML <sup>b</sup>	TL <sup>c</sup>	Source of data	Data range	Sample size	Age, years	Open access data	Research type
23	Torgersen et al (2024) [50]	CT	DL	NR	Philadelphia VA <sup>f</sup> Medical Center	01 Jan 2010-30 Dec 2017	120	• 61.1 (55.3-64.6)	• Retrospective study	
24	Wang et al (2023) [51]	Ultrasound	DL	NR	Chang Gung Memorial Hospital, Taiwan	NR	131	Mean (age range)	• Single-center study	
								• Grade 0: 9 (3-17)	• Prospective study	
								• Grade 1: 13 (10-17)	• Single-center	
								• Grade 2: 11 (4-17)		
								• Grade 3: 12 (8-17)		
25	Jeon et al (2024) [52]	CT	ML	NR	Institute of Radiation Medicine, Seoul National University Medical Research Center, Seoul National University Hospital, Seoul, Korea	Dec 2018-Dec 2021	252	• mean: 37.3 range: 18-64	• Retrospective study	
26	Piella et al (2024) [53]	Mobile phones	ML	NR	Vall d'Hebron University Hospital	NR	192	• median (IQR): 62 (50.25-71.75)	• Single-center	
27	Yoo et al (2024) [54]	CT	DL	NR	Radiologic database in our institution	Jan 2017-Jun 2021	362	• mean (SD): 37.3 (11.5) range: 18-65	• Retrospective study	
28	Zhang et al (2024) [55]	CT	DL	NR	LIDC-IDRI, NSCLC-Lung1, RIDER, VESSEL12, MIDRC-RICORD, COVID-19-Italy, and COVID-19-China	NR	986	• NR Yes	• Single-center study	
								• Retrospective study	• Multicenter	

Number	Study	Device	DL <sup>a</sup> or ML <sup>b</sup>	TL <sup>c</sup>	Source of data	Data range	Sample size	Age, years	Open access data	Research type
29	Cherchi et al (2021) [56]	Pathology	DL	NR	The University Hospital of Udine	Jan 2018-May 2019	33	• NR	No	• Retrospective study
30	Wu et al (2023) [57]	Ultrasound	DL	NR	Chang Gung Memorial Hospital	NR	276	• NR	No	• Single-center study
31	Dražinos et al (2025) [58]	Ultrasound	DL	NR	The University of Texas MD Anderson Cancer Center	Jan 2018-Jan 2019	112	• mean (SD): 51 (16.13)	No	• Single-center study
32	Kaffas et al (2025) [59]	Ultrasound	DL	NR	NR	01 Jan 2010-01 Jan 2022	403	• median (IQR): 53 (40-66)	No	• Single-center study
33	Kim et al (2025) [60]	CT	DL	NR	Asan Medical Center, University of Ulsan College of Medicine, Seoul, Republic of Korea	2001-2016	3620	• mean (SD): 31.7 (9.4)	No	• Single-center study
34	Zhang et al (2025) [61]	CT	DL	NR	The First Affiliated Hospital of Zhengzhou University	Jul 2022-May 2023	840	• mean (SD): 49.1 (11.5)	Yes	• Single-center study
35	Derstine et al (2025) [62]	CT	DL	NR	Michigan Medicine; VA	NR	1740	• mean (SD): 43.1 (12.8)	Yes	• Single-center study

Number	Study	Device	DL <sup>a</sup> or ML <sup>b</sup>	TL <sup>c</sup>	Source of data	Data range	Sample size	Age, years	Open access data	Research type
36	Corso et al (2024) [63]	Ultrasound	DL	NR	The University of Texas MD Anderson Cancer Center	NR	186	• mean (SD): 51.95 (13.4)	No	<ul style="list-style-type: none"> <li>• Prospective study</li> <li>• Multicenter</li> </ul>

<sup>a</sup>DL: deep learning.

<sup>b</sup>ML: machine learning.

<sup>c</sup>TL: transfer learning.

<sup>d</sup>MRI: magnetic resonance imaging.

<sup>e</sup>NR: No report.

<sup>f</sup>VAs: Veterans Administration.

**Table 2.** Summary of artificial intelligence (AI) performance for diagnosing hepatic steatosis (HS) based on different subgroups (number of studies or cohorts; pooled sensitivity; specificity; area under the curve [AUC]; heterogeneity [ $I^2$ , %]; Spearman correlation coefficient [for threshold effect]; and publication bias such as posttest probability positive or negative, positive likelihood ratio [LRP], and negative likelihood ratio [LRN]).

Subgroup and subgroup analysis (studies/datasets)	Pooled sensitivity (95% CI); $P$ (%)	Pooled specificity (95% CI); $P$ (%)	Summary AUC (95% CI)	Spearman correlation coefficient ( $P$ value)	Publication bias ( $P$ value)	Posttest probability positive (%)/ negative (%)	LRP	LRN
AI type								
DL <sup>a</sup> (29/32)	0.96 (0.94-0.98); 95.87	0.94 (0.91-0.95); 97.69	0.98 (0.97-0.99)	0.21 ( $P=.05$ )	.46	94/4	>10	<0.1
ML <sup>b</sup> (4/4)	0.87 (0.78-0.93); 32.63	0.88 (0.80-0.93); 63.45	0.94 (0.91-0.96)	-1 ( $P=.99$ )	.49	88/13	<10	>0.1
Reference standard								
MRI-PDFF <sup>c</sup> (7/7)	0.92 (0.86-0.95); 95.70	0.91 (0.86-0.94); 98.43	0.97 (0.95-0.98)	-0.36 ( $P=.13$ )	.15	91/8	>10	<0.1
Pathology (13/14)	0.97 (0.92-0.99); 97.86	0.92 (0.86-0.95); 85.60	0.98 (0.96-0.99)	0.12 ( $P=.02$ )	.29	92/3	>10	<0.1
Ultrasound (6/6)	0.98 (0.90-1.00); 94.32	0.96 (0.94-0.98); 85.23	0.98 (0.96-0.99)	1 ( $P=.99$ )	.21	96/2	>10	<0.1
Imaging modality								
Ultrasound (20/22)	0.96 (0.93-0.98); 94.86	0.93 (0.90-0.96); 96.16	0.98 (0.97-0.99)	0.21 ( $P=.4$ )	.50	94/4	>10	<0.1
CT <sup>d</sup> (8/9)	0.93 (0.86-0.96); 94.43	0.93 (0.87-0.96); 94.76	0.97 (0.95-0.98)	0.20 ( $P=.04$ )	.24	93/7	>10	<0.1
Pathology (4/4)	0.98 (0.91-1.00); 79.53	0.96 (0.86-0.99); 0.00	0.99 (0.98-0.99)	-1 ( $P=.99$ )	.00	96/2	>10	<0.1
TL <sup>e</sup>								
Used (9/9)	0.99 (0.96-1.00); 95.36	0.93 (0.88-0.97); 93.80	0.99 (0.98-1.00)	0.2 ( $P=.04$ )	.77	94/1	>10	<0.1
Not used (24/27)	0.93 (0.90-0.96); 84.22	0.93 (0.90-0.95); 96.71	0.98 (0.96-0.99)	0.22 ( $P=.05$ )	.53	93/7	>10	<0.1
Study design								
Single-center (25/27)	0.94 (0.91-0.96); 94.44	0.93 (0.91-0.95); 97.33	0.98 (0.96-0.99)	0.25 ( $P=.06$ )	.98	93/6	>10	<0.1
Multicenter (8/9)	0.99 (0.94-1.00); 95.26	0.92 (0.85-0.96); 82.33	0.97 (0.96-0.99)	0.47 ( $P=.22$ )	.30	92/1	>10	<0.1
Study type								
Retrospective (25/26)	0.95 (0.92-0.97); 96.58	0.95 (0.92-0.97); 98.15	0.98 (0.97-0.99)	0.39 ( $P=.15$ )	.53	95/5	>10	<0.1
Prospective (8/10)	0.97 (0.92-0.99); 0.99);	0.87 (0.84-0.89);	0.90 (0.87-0.92)	1 ( $P=.99$ )	.87	88/4	<10	<0.1

Subgroup and subgroup analysis (studies/datasets)	Pooled sensitivity (95% CI); <i>P</i> (%)	Pooled specificity (95% CI); <i>P</i> (%)	Summary AUC (95% CI)	Spearman correlation coefficient ( <i>P</i> value)	Publication bias ( <i>P</i> value)	Posttest probability positive (%)/ negative (%)	LRP	LRN
	82.76	53.89						
Data availability								
Available (9/10)	0.99 (0.96- 1.00); 97.06	0.95 (0.92- 0.97); 73.17	0.99 (0.97-0.99)	-0.5 ( <i>P</i> =.25)	.19	96/1	>10	<0.1
Unavailable (24/26)	0.92 (0.89- 0.95); 81.89	0.92 (0.89- 0.94); 96.62	0.97 (0.95-0.98)	0.09 ( <i>P</i> =.01)	.30	92/8	>10	<0.1

<sup>a</sup>DL: deep learning.<sup>b</sup>ML: machine learning.<sup>c</sup>MRI-PDFF: magnetic resonance imaging–proton density fat fraction.<sup>d</sup>CT: computed tomography.<sup>e</sup>TL: transfer learning

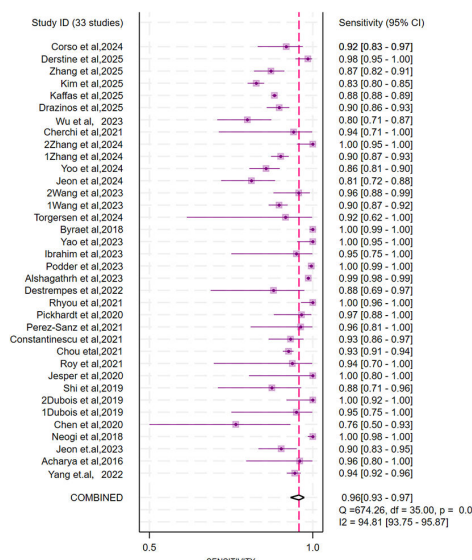
## Diagnostic Performance and Heterogeneity

Of the 36 included studies, 33 (comprising 36 datasets) satisfied the criteria for subgroup analysis. The pooled results (Figure 2) demonstrated a summary sensitivity of 0.96 (95% CI 0.93-0.97), a specificity of 0.93 (95% CI 0.91-0.95), and an AUC of 0.98 (95% CI 0.96-0.99), indicating excellent diagnostic discrimination by the AI models. Substantial heterogeneity was observed across studies ( $P>75\%$ ). The Spearman correlation coefficient (0.21,  $P=.05$ ) suggested that

threshold effects contributed minimally to overall heterogeneity. The broad 95% PI, however, indicated that differences in diagnostic thresholds were a major source of variability. No significant small-study effects were identified ( $P=.65$ ). In terms of clinical applicability, at a pretest probability of 50%, a positive AI result increased the posttest probability to 93%, whereas a negative result reduced it to 4%. Likelihood ratio scattergram analysis confirmed that the pooled estimates were located within the “confirm and exclude” quadrant (LRP >10 and LRN <0.1), underscoring the strong clinical value of AI for both confirming and excluding HS.

**Figure 2.** Diagnostic performance of artificial intelligence (AI) models for hepatic steatosis (HS) detection across 33 studies comprising 36 datasets [28-35,37,39-52,54-63]. (A) Forest plots illustrating sensitivity and specificity for the subgroup of AI applications across 33 studies with 36 datasets. (B) Summary receiver operating characteristic (SROC) curve depicting diagnostic performance of AI across 33 studies with 36 datasets, with corresponding 95% CIs. The 95% prediction region reflects the expected range of true sensitivity and specificity in future studies. (C) Bivariate boxplot illustrating the distribution and heterogeneity of AI performance across 33 studies with 36 datasets. (D) The Deeks funnel plot for evaluation of potential publication bias. (E) The Fagan nomogram depicting posttest probabilities. (F) Clinical application plot showing positive likelihood ratio (LRP) and negative likelihood ratio (LRN). LLQ: lower-left quadrant; LUQ: upper-left quadrant; RLQ: lower-right quadrant; RUQ: upper-right quadrant; SROC: summary receiver operating characteristic.

A



Study ID (33 studies)

Sensitivity (95% CI)

Study ID (33 studies)

Study ID (33 studies)

Sensitivity (95% CI)

Study ID (33 studies)

Corso et al. 2024  
Dernstine et al. 2025  
Zhang et al. 2025  
Kim et al. 2025  
Kaffas et al. 2025  
Drazinios et al. 2025  
Wu et al. 2023  
Chen et al. 2023  
Zhang et al. 2024  
Zhang et al. 2024  
Yoo et al. 2024  
Jeon et al. 2024  
2Wang et al. 2023  
1Wang et al. 2023  
Torgersen et al. 2024  
Sarkar et al. 2023  
Yao et al. 2023  
Ibrahim et al. 2023  
Podder et al. 2023  
Alshagathir et al. 2023  
Desfrempe et al. 2022  
Rhyou et al. 2021  
Pichot et al. 2020  
Pereira-Santos et al. 2021  
Constantinescu et al. 2021  
Chou et al. 2021  
Roy et al. 2021  
Jesper et al. 2020  
Shi et al. 2019  
2D'Unger et al. 2019  
1D'Unger et al. 2019  
Chen et al. 2020  
Neogi et al. 2018  
Jeon et al. 2023  
Acharya et al. 2016  
Yang et al. 2022

COMBINED

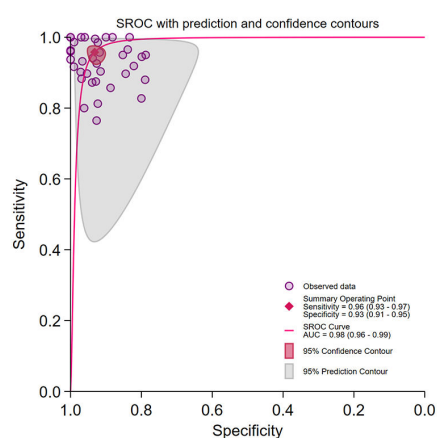
Sensitivity

COMBINED

Sensitivity

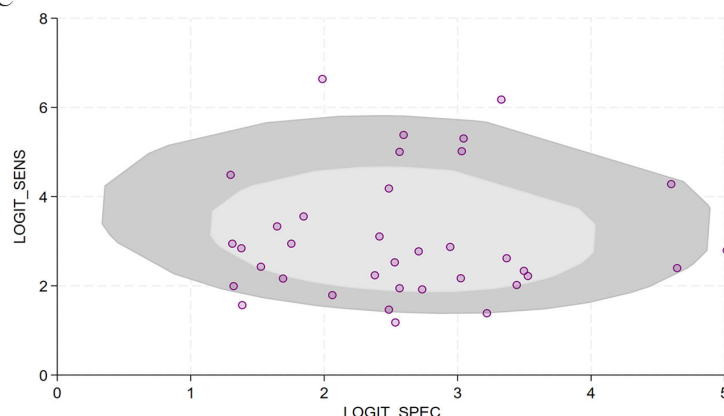
0.90 [0.83 - 0.97]  
Q = 674.26, df = 35.00, p = 0.00  
I<sup>2</sup> = 94.81 [93.75 - 95.87]

B

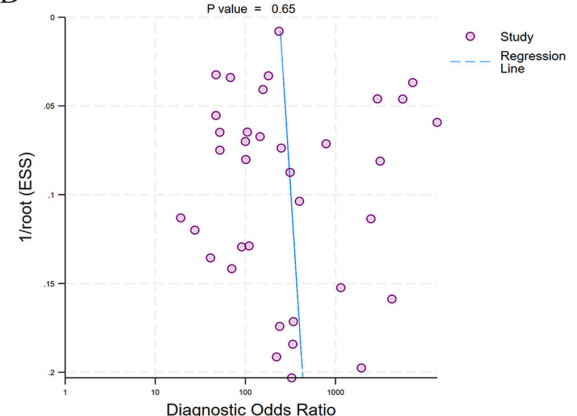


Observed data  
Summary Operating Point  
Specificity = 0.93 (0.91 - 0.95)  
SROC Curve  
AUROC = 0.96 (0.96 - 0.99)  
95% Confidence Contour  
95% Prediction Contour

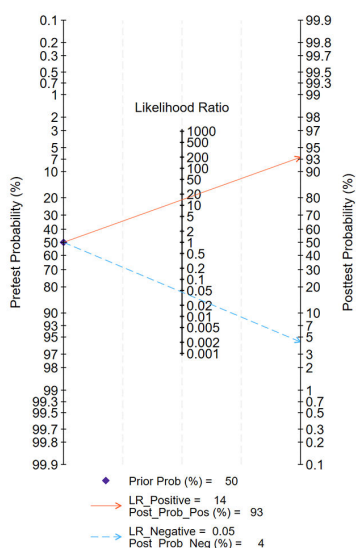
C



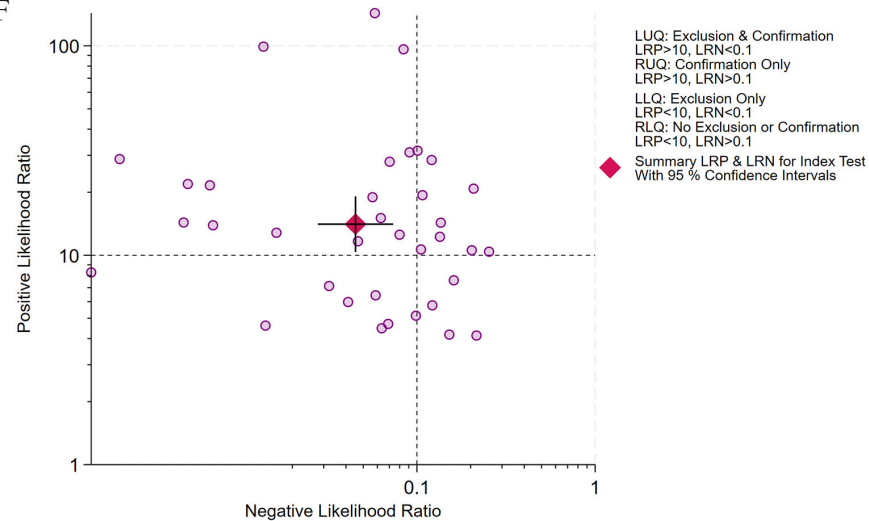
D



E



F

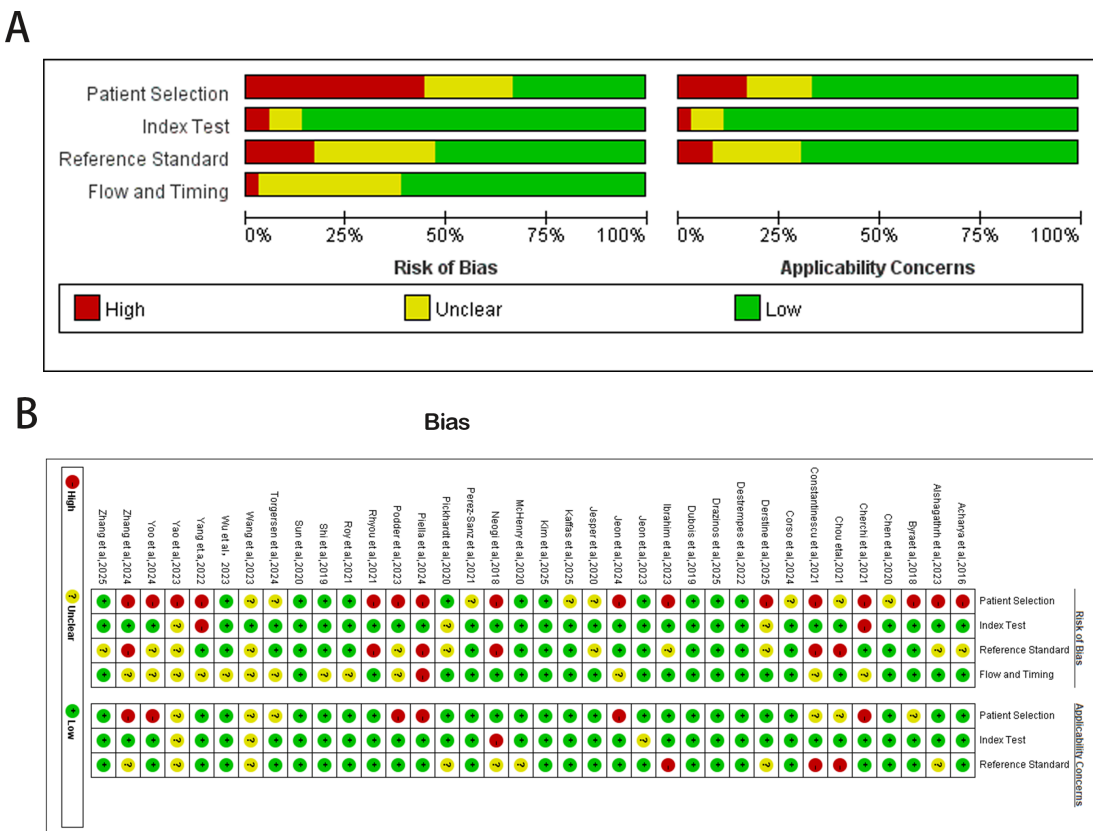


LUQ: Exclusion & Confirmation  
LRP>10, LRN<0.1  
RUQ: Confirmation Only  
LRP>10, LRN>0.1  
LLQ: Exclusion Only  
LRP<10, LRN<0.1  
RLQ: No Exclusion or Confirmation  
LRP>10, LRN>0.1  
Summary LRP & LRN for Index Test With 95 % Confidence Intervals

## Risk of Bias Assessment

The QUADAS-2 quality assessment (Figure 3) revealed that 44% (16/36) of studies exhibited a high risk of bias in the patient selection domain, primarily due to selection bias, limited representativeness of study populations, and incomplete reporting of key clinical parameters. In the Index test domain, 6% (2/36) of studies were rated as high risk, largely attributable to the absence of image quality control, subjective elements during image processing, and nonstandardized training or validation procedures. In the

**Figure 3.** Risk of bias assessment of the 36 included studies on artificial intelligence–based hepatic steatosis diagnosis using the QUADAS-2 (Quality Assessment of Diagnostic Accuracy Studies 2) tool [28-63].



## Subgroup Meta-Analyses

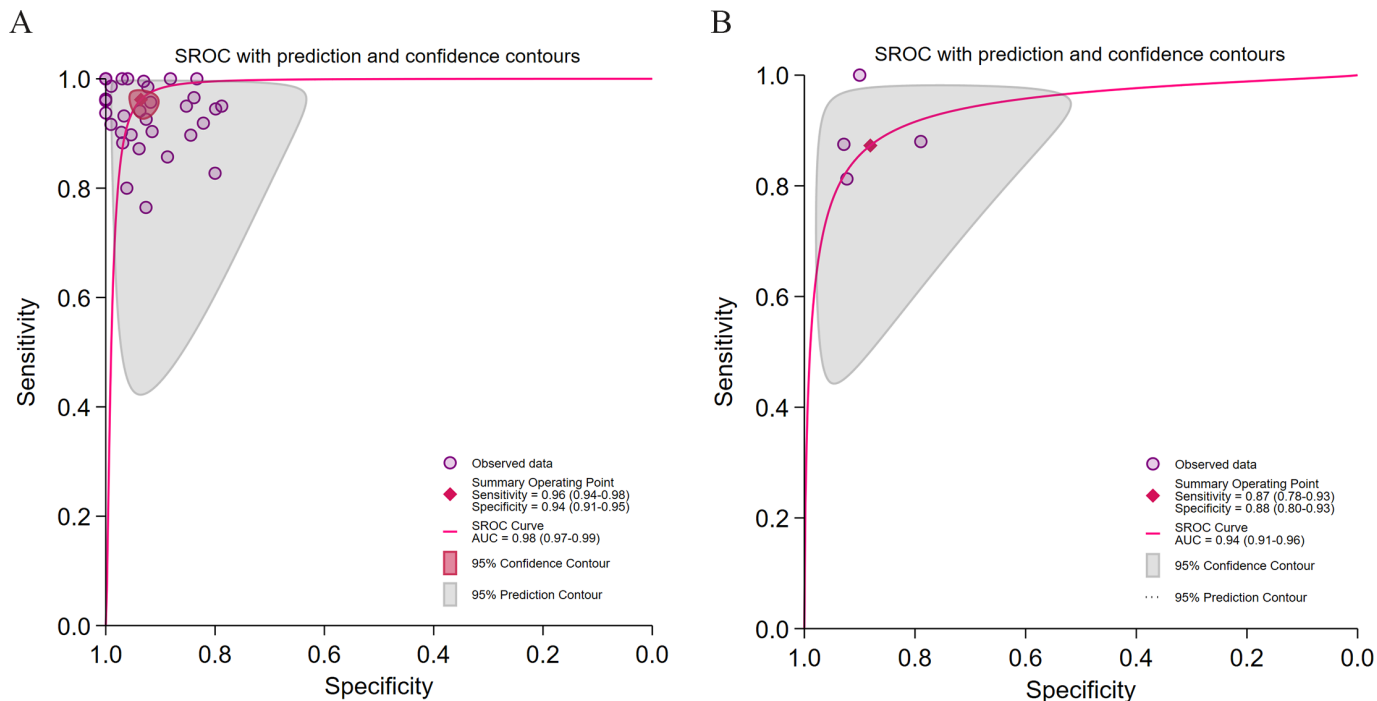
Subgroup analyses were conducted for 7 key variables (Figures S1-S16 in [Multimedia Appendix 1](#)), with diagnostic performance interpreted relative to clinical applicability thresholds (LRP >10 for strong rule-in capability; LRN <0.1 for strong rule-out capability).

## Algorithm Type

As shown in [Figure 4 A-B](#), the DL models demonstrated significantly higher diagnostic accuracy than ML

reference standard domain, 17% (6/36) of studies demonstrated a high risk of bias, most commonly due to deviations from gold-standard reference methods, unclear blinding procedures, or incomplete pathological sampling information. The flow and timing domain exhibited unclear risk in 36% (14/36) of studies, often due to insufficient reporting on patient inclusion pathways and the interval between image acquisition and diagnostic confirmation. These methodological limitations may contribute to an overestimation of AI model performance in real-world clinical practice.

**Figure 4.** Diagnostic performance stratified by algorithm type for hepatic steatosis (HS) detection. (A) Summary receiver operating characteristic (SROC) curve for deep learning (DL) algorithms in 29 studies [28-33,37,39-43,45-51,54-63] comprising 32 datasets; (B) SROC curve for machine learning (ML) algorithms in 4 studies [34,35,44,52] comprising 4 datasets.

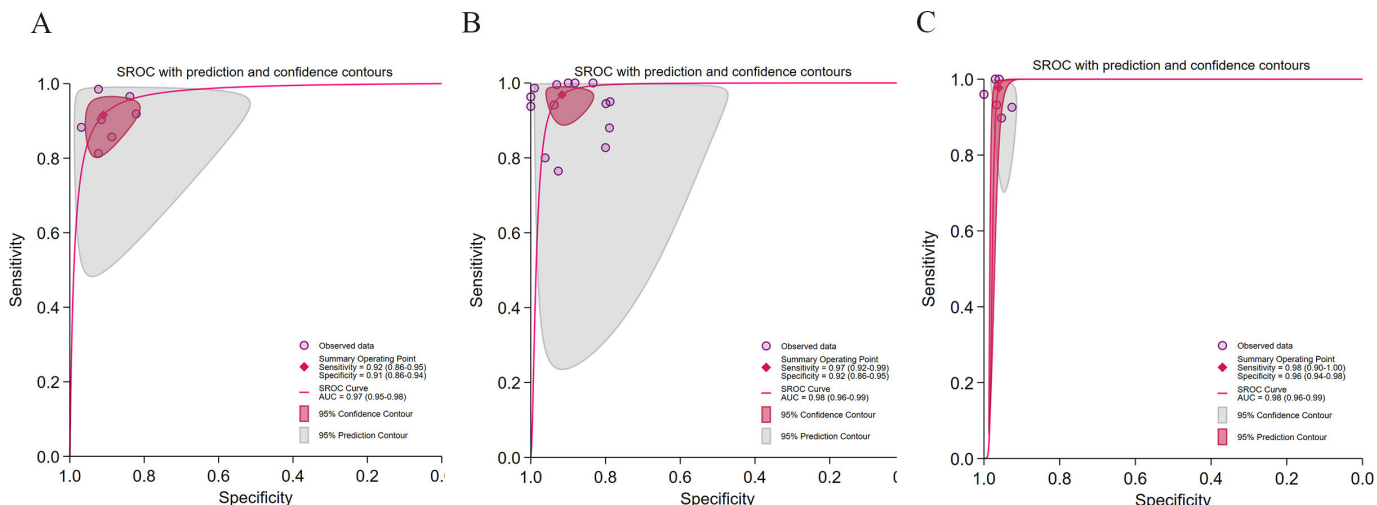


## Reference Standard

As shown in **Figure 5 A-C**, studies using ultrasound and histopathology as reference standards achieved comparable AUCs (both were 0.98) with ideal likelihood ratios, although ultrasound-based models exhibited higher pooled sensitivity and specificity (0.98 and 0.96, respectively) than histopathology-based models (0.97 and 0.92). The ultrasound subgroup showed a perfect threshold effect (Spearman=1;

$P=.99$ ), indicating well-defined diagnostic criteria that may be subjectively constrained. The histopathology subgroup exhibited a minimal threshold effect (Spearman=0.12;  $P=.02$ ), suggesting that interstudy variations in sample handling and scoring could significantly influence model performance. The MRI-PDFF subgroup achieved a comparable AUC (0.97) but demonstrated very high heterogeneity ( $I^2 > 95\%$ ), limiting result stability.

**Figure 5.** Diagnostic performance stratified by reference standard for hepatic steatosis (HS) detection. (A) Summary receiver operating characteristic (SROC) curve for magnetic resonance imaging–proton density fat fraction (MRI-PDFF) in 7 studies [30,42,52,54,59,62,63] comprising 7 datasets; (B) SROC curve for pathology in 13 studies [28,32,33,35,41,43-46,49,56,57,60] comprising 14 datasets; (C) SROC curve for ultrasound in 6 studies [29,31,39,40,48,58] comprising 6 datasets.



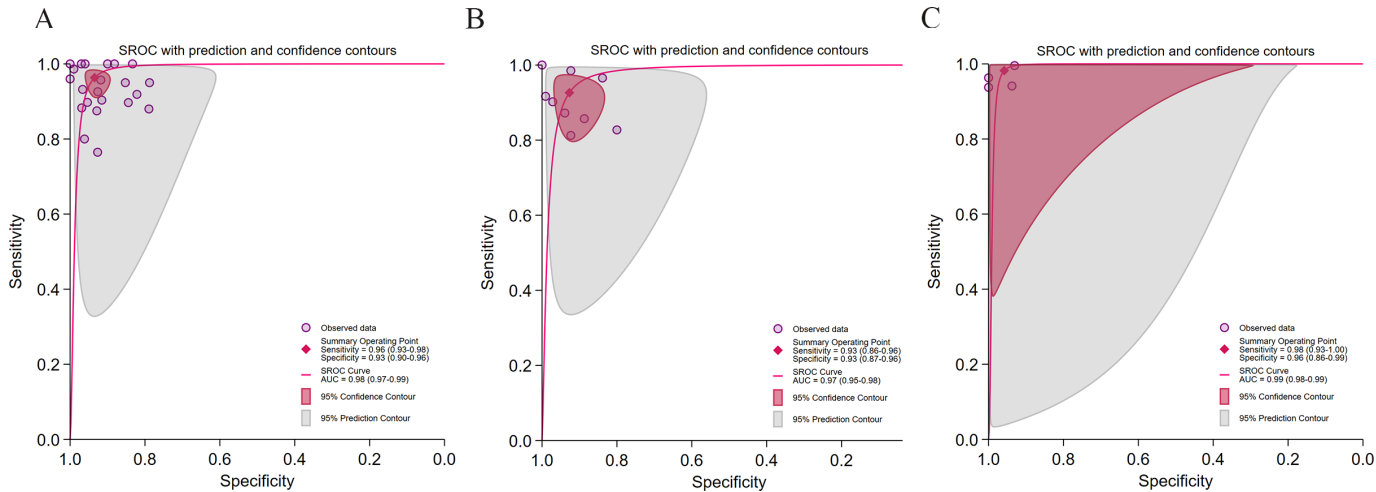
## Imaging Modality

As shown in **Figure 6 A-C**, histopathology-based models achieved the highest diagnostic performance (AUC=0.99)

with no detectable heterogeneity, suggesting robust and consistent results. However, significant publication bias was identified ( $P<.001$ ), implying potential preferential publication of high-performing studies. AI models based on

ultrasound and CT achieved comparable accuracy (AUC: 0.98 vs 0.97), though both exhibited marked heterogeneity ( $I^2 >94\%$ ). Only the CT subgroup showed a negligible threshold effect (Spearman=0.20;  $P=.04$ ).

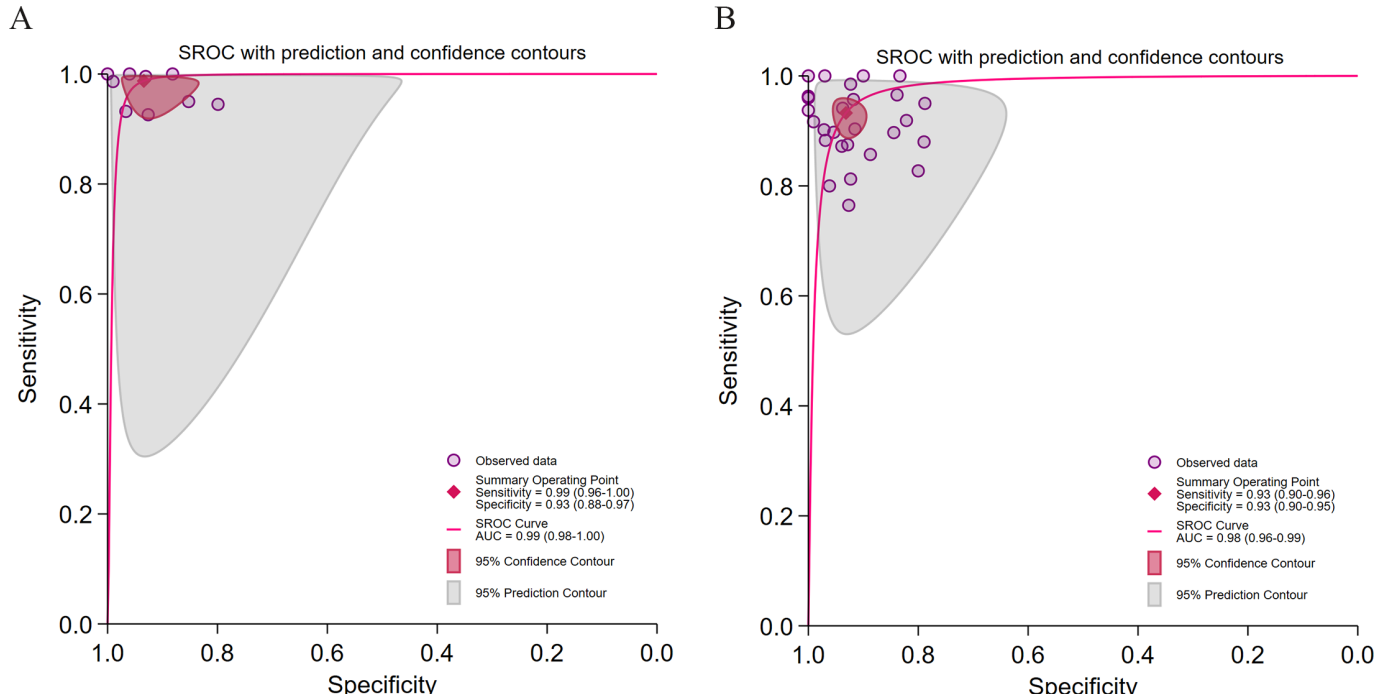
**Figure 6.** Diagnostic performance stratified by imaging modality for hepatic steatosis (HS) detection. (A) Summary receiver operating characteristic (SROC) curve for ultrasound imaging in 20 studies [29-35,39,40,43-45,47-49,51,57-59,63] comprising 22 datasets; (B) SROC curve for computed tomography (CT) imaging in 8 studies [42,50,52,54,55,60-62] comprising 9 datasets; (C) SROC curve for pathology imaging in 4 studies [37, 41,46,56] comprising 4 datasets.



## Application of TL

As shown in the figure **Figure 7A-B** models employing TL achieved higher pooled sensitivity (0.99 vs 0.93) and stronger rule-out capability (LRN: 0.01 vs 0.07). No significant publication bias was detected in either subgroup ( $P >.05$ ).

**Figure 7.** Diagnostic performance of transfer learning (TL) for hepatic steatosis (HS) detection. (A) Summary receiver operating characteristic (SROC) curve for studies employing TL in 9 studies [28,39,40,43,45-49] comprising 9 datasets; (B) SROC curve for studies not employing TL in 24 studies [29-35,37,41,42,44,50-52,54-63] comprising 26 datasets.



## Study Design

As shown in **Figure 8A-B**, multicenter studies demonstrated superior sensitivity (0.99 vs 0.94) and lower heterogeneity

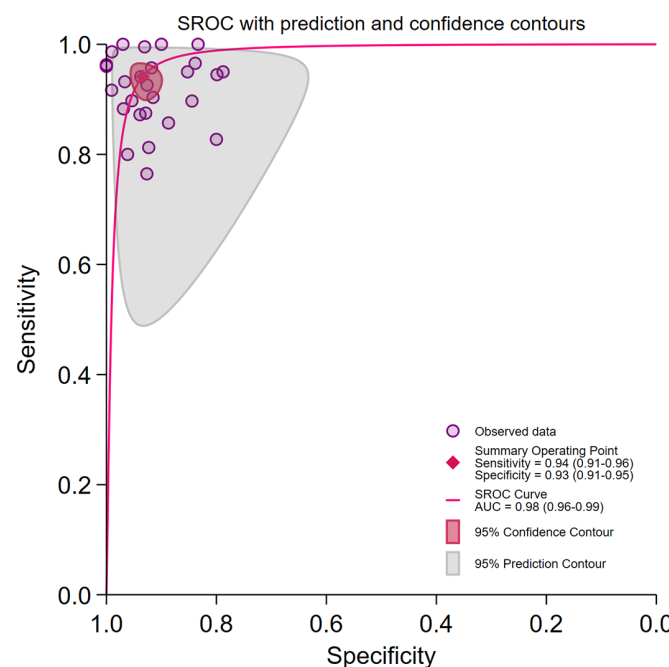
Nevertheless, both demonstrated considerable heterogeneity ( $I^2 >84\%$ ) and mild threshold effects (Spearman=0.20 vs 0.22;  $P=.04$  vs .05), reflecting the influence of interdomain data discrepancies.

( $I^2=82.33\%$ ), indicating greater generalizability and stronger rule-out potential (LRN: 0.01 vs 0.06). In contrast, single-center studies exhibited marginally higher specificity (0.93

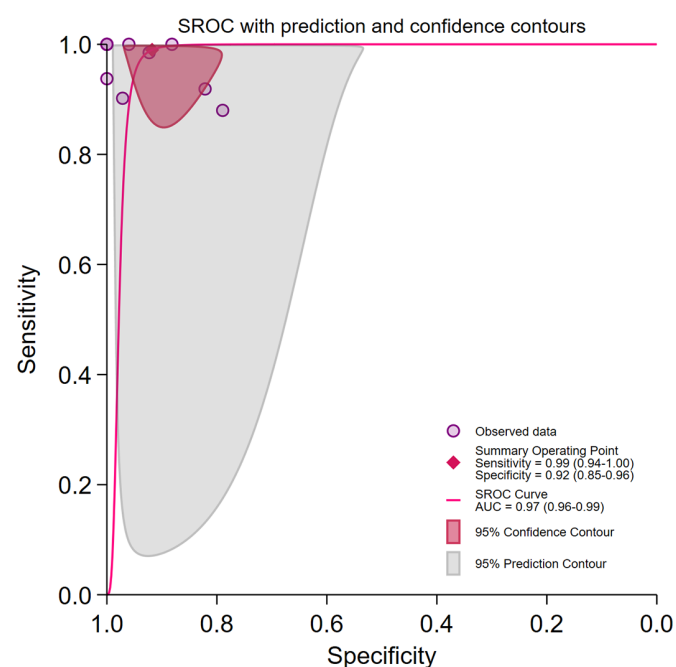
vs 0.92) but very high heterogeneity ( $P > 94\%$ ), suggesting limited external validity.

**Figure 8.** Diagnostic performance of different research designs for hepatic steatosis (HS) detection. (A) Summary receiver operating characteristic (SROC) curve for single-center studies in 25 studies [28-35,39-42,45-47,50-52,54,56-61] with 26 datasets; (B) SROC curve for multicenter studies in 8 studies [37,43,44,48,49,55,62,63] with 9 datasets.

A



B



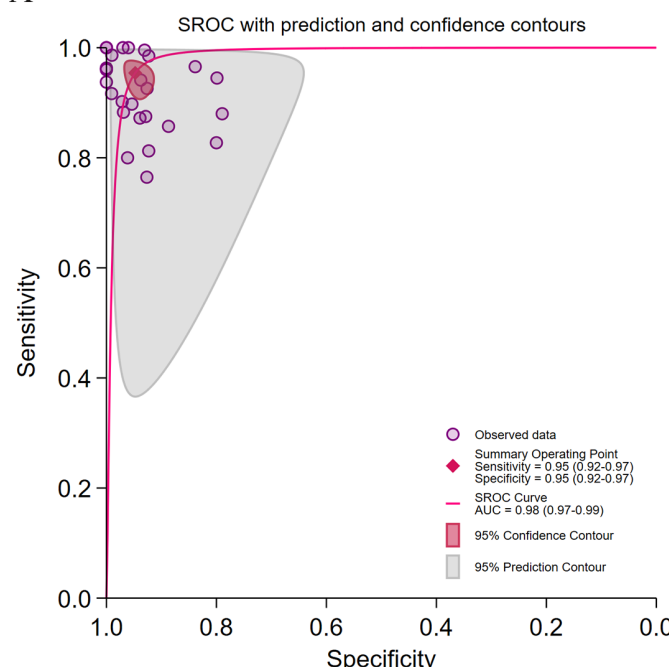
## Study Type

As shown in **Figure 9 A-B**, retrospective studies achieved higher overall accuracy (AUC: 0.98 versus 0.90) and stronger rule-in ability (LRP: 9.5 versus 8.8), though with significant

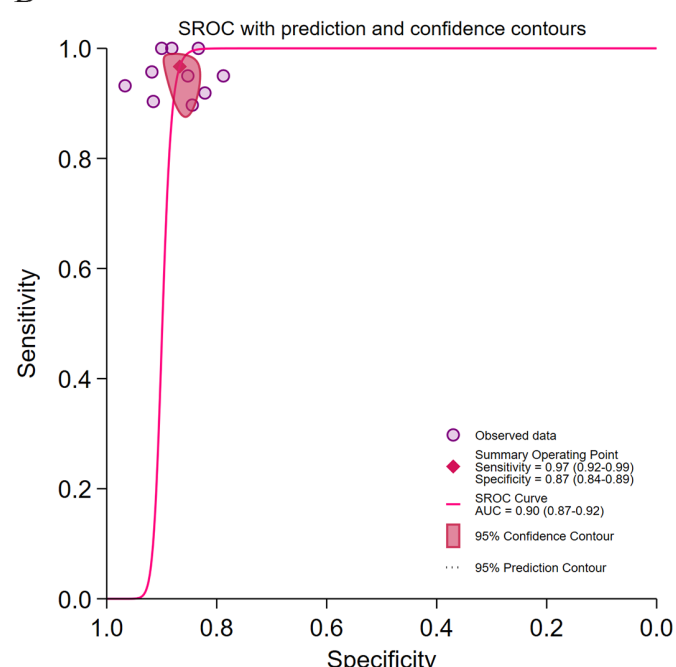
heterogeneity ( $P > 96\%$ ). Prospective studies, which can better reflect clinical reality, were affected by a perfect threshold effect (Spearman=1) and exhibited weaker rule-in performance (LRP<10).

**Figure 9.** Diagnostic performance of different research types for hepatic steatosis (HS) detection. (A) Summary receiver operating characteristic (SROC) curve for retrospective studies in 25 [28,29,31,32,34,37,41-46,48,50,52,54-62] studies with 26 datasets; (B) SROC curve for prospective studies in 8 studies with 9 datasets. AUC: area under curve.

A



B

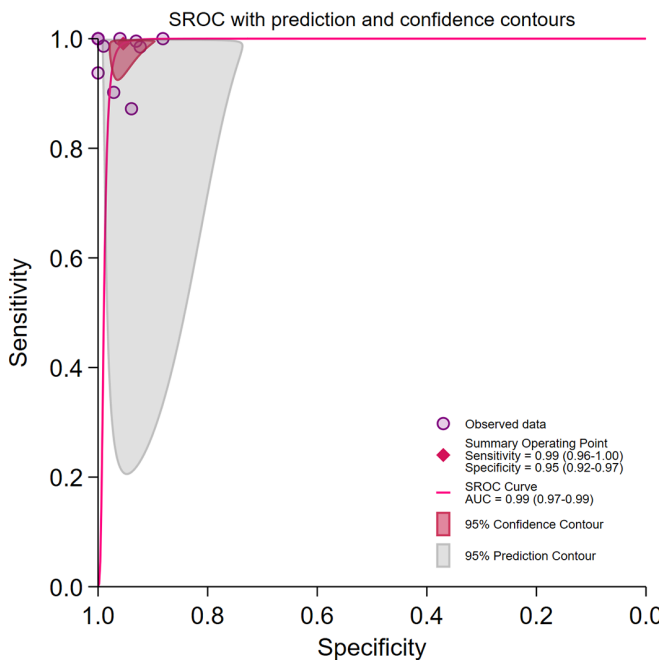


## Data Accessibility

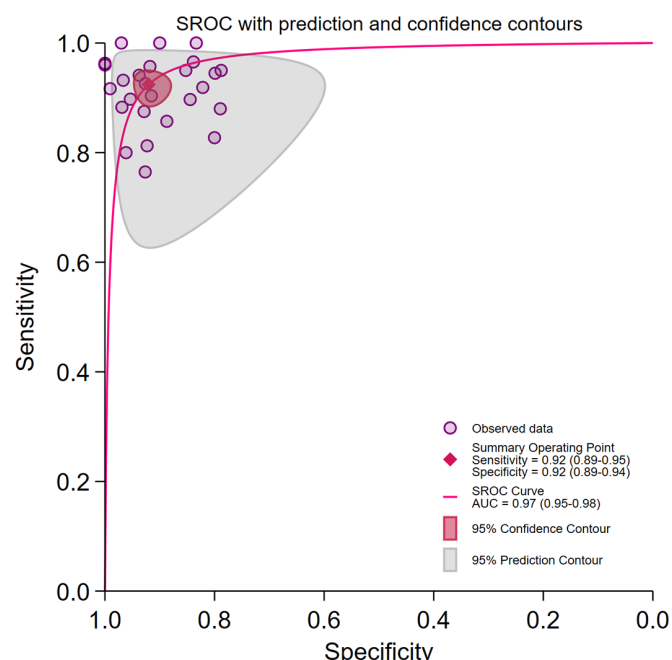
As shown in Figure 10A-B studies using publicly available datasets ( $n=9$ ) achieved superior diagnostic accuracy ( $AUC=0.99$ ) and stronger clinical applicability (LRP=9.6;

**Figure 10.** Diagnostic performance of data availability for hepatic steatosis (HS) detection. (A) Summary receiver operating characteristic (SROC) curve for studies with available data in 9 studies [37,43,45,46,48,49,55,61,62] with 10 datasets; (B) SROC curve for studies with unavailable data in 24 studies [28-35,38-42,44,47,50-52,54,56-60,63] with 25 datasets.

A



B



Subgroup definitions are detailed in the methods section. Heterogeneity was categorized as follows:  $I^2<50\%$  low heterogeneity, 50%-75% moderate heterogeneity, and  $>75\%$  high heterogeneity.

## Discussion

### Principal Findings

This meta-analysis of 36 studies demonstrates the superior diagnostic performance of AI in identifying HS, yielding a pooled  $AUC$  of 0.98, surpassing that of conventional ultrasound, CT, and MRI, whose pooled  $AUC$ s were 0.93, 0.975, and 0.97, respectively [64-66]. These findings underscore AI's potential to overcome the inherent physical constraints of individual imaging techniques, thereby establishing it as a versatile and adaptive diagnostic approach. This capability carries considerable clinical significance, providing a strong rationale for further meta-analyses dedicated to AI-based diagnostic technologies and informing the development of flexible, context-specific clinical applications. By optimizing the use of the most accessible and cost-effective diagnostic resources, AI could markedly broaden the availability of early HS screening across diverse health care settings.

Although the encouraging performance of AI in diagnosing HS is promising, interpretation of these findings must

be tempered by a critical appraisal of the methodological limitations underlying this research. Our analysis revealed substantial heterogeneity ( $I^2>75\%$ ) and a high overall risk of bias among included studies, particularly within the patient selection domain, where 44% (16/36) were judged to be at high risk. A major limitation lies in the predominance of retrospective, single-center designs (25/36, 69%). Such studies typically develop and validate models within controlled, idealized data environments, meaning that reported metrics may reflect "best-case scenarios" rather than true clinical performance across diverse devices, operators, and patient populations in routine practice. Moreover, independent external validation and multicenter prospective trials remain notably scarce, severely limiting the assessment of these models' generalizability. Therefore, while existing evidence underscores AI's considerable potential in HS diagnosis, the current body of research remains insufficient to justify its widespread clinical adoption. Bridging the translational gap from high-performing algorithms to reliable, universally applicable clinical tools thus remains a substantial challenge.

Subgroup analyses provide valuable insights for optimizing AI model design and informing clinical integration. DL-based models demonstrate exceptionally high specificity in diagnosing HS, offering a distinct clinical advantage by reducing unnecessary liver biopsies. However, these models require higher-quality data annotation and greater

computational resources. Model performance was also closely associated with the reference standard and imaging modality used. Systems using histopathological images as input achieved the highest diagnostic accuracy. Nevertheless, their clinical applicability is restricted by procedural invasiveness and sampling error [67]. The AI-assisted whole-slide analysis model proposed by Roy et al [37] improves quantitative consistency but faces practical barriers related to cost and patient acceptance.

The choice of imaging modality inherently involves trade-offs between diagnostic accuracy, accessibility, and cost. MRI-PDFF, while providing precise, noninvasive quantification, is affected by confounders such as iron overload, edema, and concurrent pathologies [7], and its high cost limits use in primary care. Ultrasound remains the most accessible and economical option but suffers from operator dependency, reduced sensitivity for mild steatosis, limited penetration in obese individuals [68,69], and suboptimal accuracy in detecting fibrosis [70]. AI integration could mitigate these limitations by standardizing acquisition and interpretation, though at the cost of increased system complexity and computational demand. CT achieves a sensitivity and specificity of 0.93 but is constrained by ionizing radiation exposure and potential interference from iodine-based contrast agents [71]. The dual-energy CT 3D nnU-Net model developed by Yoo et al [54] achieved an AUC of 0.97 for distinguishing steatotic from normal tissue, yet its clinical application is constrained by limited equipment availability.

To optimize model performance and data use, TL has been widely adopted, an especially valuable strategy given the substantial costs associated with medical data annotation. Nonetheless, the effectiveness of TL depends critically on the degree of similarity between the source and target domains; substantial domain discrepancies may lead to “negative transfer,” as illustrated by sensitivity variations of up to 10% in the Inception-v3 model reported by Constantinescu et al [40]. To address this limitation, emerging approaches such as adversarial domain adaptation frameworks have achieved near-human classification accuracy on heterogeneous MRI datasets [72]. Similarly, hybrid pretraining strategies [73] and federated learning techniques have reached up to 99% of the performance attained through centralized training [74]. These approaches enhance model robustness while effectively addressing data privacy and heterogeneity.

Beyond algorithmic optimization, the real-world implementation of AI is profoundly influenced by study design and data governance. Retrospective studies, which constituted the majority (25/36, 69%) of the included reports, demonstrated significantly higher performance than prospective studies (AUC: 0.98 vs 0.94), likely reflecting the high-quality and well-curated imaging data typically available in retrospective cohorts. In contrast, prospective designs more faithfully capture real-world clinical workflows but are inherently subject to operational variability, such as inconsistent imaging protocols and unpredictable patient factors, thereby leading to attenuated performance.

Furthermore, data governance and accessibility are pivotal in determining model generalizability. Multicenter collaborations and data sharing can improve generalizability and reproducibility, though they require standardized imaging protocols, increased logistical coordination, and greater resource investment, posing feasibility challenges in resource-limited settings. Moreover, access to medical data for AI development remains hindered by privacy regulations, institutional policies, and technical interoperability barriers. Privacy-preserving strategies, such as federated learning, offer promising solutions by enabling multi-institutional collaboration without direct data exchange, albeit at the cost of increased computational demands and system complexity. It should also be noted that publicly available datasets may not fully represent the clinical heterogeneity encountered in real-world practice, thereby introducing potential selection bias. These factors, while critical for improving AI performance, also contribute substantially to heterogeneity, underscoring the necessity of comprehensive external validation and context-specific adaptation before large-scale clinical implementation.

## Expanding Role in HS Management

The use of AI extends beyond diagnostic precision to encompass the comprehensive management of HS. Accumulating evidence indicates that AI not only enables accurate quantification of hepatic fat but also integrates radiomic, pathological, and clinical data to facilitate fibrosis staging, predict HCC risk, assess posttransplant survival, and stratify cardiovascular complications. For instance, a VGG16-based ultrasound model outperformed human interpretation in classifying borderline cases [75]. The integration of macrogenomic sequencing with ML has proven effective for the differential diagnosis of HS in obese pediatric populations [76]. Similarly, an ML model based on MRI-derived liver fat quantification markedly improved diagnostic accuracy for liver fibrosis [77]. AI-powered digital pathology platforms reduce the inherent subjectivity of conventional histological assessment [78], while DL-based radiomics facilitates the identification of critical pathological features such as microvascular invasion [79]. A DL algorithm demonstrated 99% accuracy in predicting postliver transplantation survival [80]. In the context of MAFLD-related complications, AI algorithms have been employed to accurately identify affected patients from electronic health records, revealing type 2 diabetes mellitus as a significant predictor of all-cause mortality (hazard ratio: 1.36) [81]. Moreover, a dual model combining tongue imaging with clinical indicators achieved precise prediction of coronary heart disease risk among patients with fatty liver [82]. The foregoing advances signal a diagnostic paradigm shift in HS management from a traditional “liver-centric” approach towards a “patient-centric” model of multi-system risk management, paving the way for early intervention and personalized therapy.

In summary, the advantages of AI in HS diagnosis are threefold as follows:

1. Enhanced early detection: DL models can detect subclinical pathological alterations, including hepatic

fat infiltration below 5%, thereby reducing diagnostic subjectivity and improving reproducibility [43,45,83].

2. Standardized quantitative analysis: End-to-end, pixel-level segmentation enables automated calculation of HS, minimizing reliance on manual interpretation and potentially substituting for histopathological assessment in resource-constrained settings.
3. Longitudinal predictive modeling: The integration of time-series radiomic and metabolomic features facilitates the construction of individualized models predicting cirrhosis progression and MAFLD onset within 3 years, providing actionable insights for precision treatment planning.

### **Challenges and a Phased Implementation Framework**

Despite its promising outlook, the widespread clinical adoption of AI in HS management faces multiple challenges. Technically, data heterogeneity, stemming from variations in imaging quality [84], scanner types, and reference standard thresholds, impedes the development of universally robust and generalizable models. Many high-performing algorithms are derived from single-center, retrospective datasets (eg, Yang et al [22], n=50, Beijing) with limited demographic diversity, thereby compromising their external validity and real-world applicability. Moreover, most existing models primarily focus on imaging biomarkers for fat quantification without adequately elucidating the complex pathophysiological interplay among steatosis, metabolic comorbidities, and fibrosis, limiting both clinical interpretability and holistic disease assessment.

From a clinical integration perspective, the transition from algorithmic development to real-world deployment necessitates careful consideration of workflow compatibility, device dependency, and cost-effectiveness. Lightweight AI models hold promise for incorporation into primary care ultrasound systems, facilitating large-scale population screening, whereas more advanced MRI- or CT-based models may be more appropriately implemented in tertiary medical centers. The overarching objective is seamless integration into existing clinical workflows, ensuring that AI serves as an assistive, rather than disruptive, technology that streamlines radiological practice, conserves clinician time, and enhances diagnostic efficiency [85]. Furthermore, issues concerning data privacy [86], algorithmic bias [87], and accountability [88] lack clear regulatory frameworks.

From a global health perspective, the clinical use of AI in HS diagnosis varies according to resource availability. To promote both efficiency and equity in HS diagnosis and management, a phased implementation framework is proposed:

1. Tiered deployment in specific scenarios: in resource-limited settings, lightweight AI systems can be paired with portable ultrasound to enable cost-effective community screening and early detection. Suspected cases may then be referred to higher-level hospitals for precise stratified diagnosis (eg, MRI-PDFF), thereby optimizing resource allocation and minimizing

unnecessary biopsies. In high-resource environments, AI-driven automated image processing facilitates accurate fat quantification and disease staging, forming a synergistic diagnostic-therapeutic feedback loop.

2. Establish cross-institutional collaborative data platforms: the adoption of federated learning and related technologies can enhance data diversity while ensuring privacy protection. Such approaches enable robust model development based on heterogeneous real-world data, mitigate model bias and validation gaps, eliminate the need for centralized storage of sensitive information, and provide the foundation for scalable, privacy-preserving deployment.
3. Transition from standalone tools to integrated management platforms: the ultimate objective is to advance AI from a single-function diagnostic aid to a comprehensive, multi-task management system. By synchronously quantifying steatosis, assessing fibrosis, and evaluating inflammatory markers through multimodal data integration. Incorporating these outputs directly into clinical decision-making workflows, AI could evolve from diagnostic assistance to intelligent, holistic disease management.

### **Limitations in the Literature**

Several limitations warrant cautious interpretation. First, considerable methodological and clinical heterogeneity was observed across the included studies, constraining the reliability of the conclusions. Despite extensive subgroup analyses, variability arising from differences in patient characteristics, imaging equipment, and diagnostic thresholds could not be fully addressed. This residual heterogeneity undermines the robustness of pooled estimates and suggests the influence of unmeasured factors affecting AI performance.

Second, the analysis was limited by methodological shortcomings inherent in the primary studies. Inadequate reporting of key patient characteristics hindered subgroup analyses by disease etiology, particularly distinguishing pure MAFLD from mixed forms, a critical gap given the potential impact of comorbidities on diagnostic accuracy. Furthermore, wide variation in AI architectures and the limited number of comparable models precluded meaningful comparisons across technical approaches, leaving the effect of architectural design on diagnostic performance unclear.

Third, the generalizability and real-world applicability of the findings remain limited. Most studies were retrospective, single-center designs prone to selection bias, with scarce external or temporal validation. Thus, the high-performance metrics reported may represent an idealized best-case scenario rather than outcomes achievable in prospective clinical settings.

Additionally, although our restriction to peer-reviewed full-text publications ensured a baseline level of methodological rigor, the exclusion of relevant preprints and gray literature may have introduced publication bias. Such selective inclusion likely favored studies reporting positive outcomes, potentially leading to overestimated performance

measures. Moreover, key practical factors, such as computational burden, workflow integration, and technical expertise, could not be quantitatively evaluated, despite their importance for real-world implementation.

## Conclusions

This meta-analysis highlights the substantial diagnostic potential of AI, particularly DL, in assessing HS. Its key contribution lies in establishing a unified, imaging-modality-independent analytical framework that provides comprehensive evidence beyond the constraints of individual imaging techniques. Nonetheless, these results reflect technical

promise rather than confirmed clinical use. The translation from high-performing algorithms to reliable clinical tools remains hindered by performance heterogeneity, retrospective study designs, and insufficient external validation. While the technological foundation of AI in HS is encouraging, clinical maturity has yet to be achieved. Bridging this translational gap will require prospective multicenter studies, standardized reporting protocols, and rigorous external validation. Ultimately, successful clinical adoption will depend on demonstrating not only algorithmic robustness but also tangible improvements in patient outcomes and workflow efficiency across real-world health care settings.

## Funding

This work was supported by the Science and Technology Research Program of Jilin Provincial Department of Education (No. JKH20250664KJ). The sponsor participated in the preliminary design phase and guided the selection of research methodologies. However, the sponsor did not participate in subsequent data collection, analysis, interpretation of results, or the preparation of this manuscript.

## Data Availability

The datasets generated and analyzed during the current study are available from the corresponding author upon reasonable request.

## Authors' Contributions

Conceptualization: JS  
Data curation: JS and JL  
Formal analysis: YL  
Funding acquisition: DL  
Investigation: JL and HC  
Methodology: DL  
Project administration: JZ  
Resources: JZ  
Software: JS  
Supervision: DL and RD  
Validation: JS  
Visualization: HC  
Writing – original draft: JS  
Writing – review & editing: JZ

All authors commented on a previous version of the manuscript. All authors read and approved the final manuscript.

## Conflicts of Interest

None declared.

## Multimedia Appendix 1

Retrieval strategy, and Forest plots, bivariate boxplots, Deeks' funnel plots, Fagan's nomogram plots, and clinical application plots for each subgroup analysis.

[[DOCX File \(Microsoft Word File\), 9783 KB-Multimedia Appendix 1](#)]

## Checklist 1

PRISMA-DTA checklist.

[[PDF File \(Adobe File\), 139 KB-Checklist 1](#)]

## Checklist 2

QUADAS-2 checklist.

[[XLSX File \(Microsoft Excel File\), 31 KB-Checklist 2](#)]

## References

1. Unalp-Arida A, Ruhl CE. Prevalence of metabolic dysfunction-associated steatotic liver disease and fibrosis defined by liver elastography in the United States using national health and nutrition examination survey 2017-March 2020 and

August 2021-August 2023 data. *Hepatology*. Nov 1, 2025;82(5):1256-1273. [doi: [10.1097/HEP.0000000000001211](https://doi.org/10.1097/HEP.0000000000001211)] [Medline: [39724144](#)]

2. Riazi K, Azhari H, Charette JH, et al. The prevalence and incidence of NAFLD worldwide: a systematic review and meta-analysis. *Lancet Gastroenterol Hepatol*. Sep 2022;7(9):851-861. [doi: [10.1016/S2468-1253\(22\)00165-0](https://doi.org/10.1016/S2468-1253(22)00165-0)] [Medline: [35798021](#)]

3. Eslam M, Newsome PN, Sarin SK, et al. A new definition for metabolic dysfunction-associated fatty liver disease: an international expert consensus statement. *J Hepatol*. Jul 2020;73(1):202-209. [doi: [10.1016/j.jhep.2020.03.039](https://doi.org/10.1016/j.jhep.2020.03.039)] [Medline: [32278004](#)]

4. Gofton C, Upendran Y, Zheng MH, George J. MAFLD: how is it different from NAFLD? *Clin Mol Hepatol*. Feb 2023;29(Suppl):S17-S31. [doi: [10.3350/cmh.2022.0367](https://doi.org/10.3350/cmh.2022.0367)] [Medline: [36443926](#)]

5. Younossi ZM, Golabi P, Paik JM, Henry A, Van Dongen C, Henry L. The global epidemiology of nonalcoholic fatty liver disease (NAFLD) and nonalcoholic steatohepatitis (NASH): a systematic review. *Hepatology*. Apr 1, 2023;77(4):1335-1347. [doi: [10.1097/HEP.0000000000000004](https://doi.org/10.1097/HEP.0000000000000004)] [Medline: [36626630](#)]

6. Younossi ZM, Kalligeros M, Henry L. Epidemiology of metabolic dysfunction-associated steatotic liver disease. *Clin Mol Hepatol*. Feb 2025;31(Suppl):S32-S50. [doi: [10.3350/cmh.2024.0431](https://doi.org/10.3350/cmh.2024.0431)] [Medline: [39159948](#)]

7. Wong VWS, Ekstedt M, Wong GLH, Hagström H. Changing epidemiology, global trends and implications for outcomes of NAFLD. *J Hepatol*. Sep 2023;79(3):842-852. [doi: [10.1016/j.jhep.2023.04.036](https://doi.org/10.1016/j.jhep.2023.04.036)] [Medline: [37169151](#)]

8. Starekova J, Hernando D, Pickhardt PJ, Reeder SB. Quantification of liver fat content with CT and MRI: state of the art. *Radiology*. Nov 2021;301(2):250-262. [doi: [10.1148/radiol.2021204288](https://doi.org/10.1148/radiol.2021204288)] [Medline: [34546125](#)]

9. Leporq B, Ratiney H, Pilleul F, Beuf O. Liver fat volume fraction quantification with fat and water T1 and T 2\* estimation and accounting for NMR multiple components in patients with chronic liver disease at 1.5 and 3.0 T. *Eur Radiol*. Aug 2013;23(8):2175-2186. [doi: [10.1007/s00330-013-2826-x](https://doi.org/10.1007/s00330-013-2826-x)] [Medline: [23588583](#)]

10. Bedogni G, Bellentani S, Miglioli L, et al. The fatty liver index: a simple and accurate predictor of hepatic steatosis in the general population. *BMC Gastroenterol*. Nov 2, 2006;6:33. [doi: [10.1186/1471-230X-6-33](https://doi.org/10.1186/1471-230X-6-33)] [Medline: [17081293](#)]

11. Lee JH, Kim D, Kim HJ, et al. Hepatic steatosis index: a simple screening tool reflecting nonalcoholic fatty liver disease. *Dig Liver Dis*. Jul 2010;42(7):503-508. [doi: [10.1016/j.dld.2009.08.002](https://doi.org/10.1016/j.dld.2009.08.002)] [Medline: [19766548](#)]

12. Kotronen A, Peltonen M, Hakkilainen A, et al. Prediction of non-alcoholic fatty liver disease and liver fat using metabolic and genetic factors. *Gastroenterol*. Sep 2009;137(3):865-872. [doi: [10.1053/j.gastro.2009.06.005](https://doi.org/10.1053/j.gastro.2009.06.005)] [Medline: [19524579](#)]

13. Dasarathy S, Dasarathy J, Khiyami A, Joseph R, Lopez R, McCullough AJ. Validity of real time ultrasound in the diagnosis of hepatic steatosis: a prospective study. *J Hepatol*. Dec 2009;51(6):1061-1067. [doi: [10.1016/j.jhep.2009.09.001](https://doi.org/10.1016/j.jhep.2009.09.001)] [Medline: [19846234](#)]

14. Cho Y. Hidden burden of alcohol use disorder in MASLD and MetALD: clinical and nomenclatural implications. *Gut Liver*. Sep 15, 2025;19(5):637-638. [doi: [10.5009/gnl250414](https://doi.org/10.5009/gnl250414)] [Medline: [40947954](#)]

15. Lin H, Zhang X, Li G, Wong GLH, Wong VWS. Epidemiology and clinical outcomes of metabolic (dysfunction)-associated fatty liver disease. *J Clin Transl Hepatol*. Dec 28, 2021;9(6):972-982. [doi: [10.14218/JCTH.2021.00201](https://doi.org/10.14218/JCTH.2021.00201)] [Medline: [34966660](#)]

16. Stefan N, Yki-Järvinen H, Neuschwander-Tetri BA. Metabolic dysfunction-associated steatotic liver disease: heterogeneous pathomechanisms and effectiveness of metabolism-based treatment. *Lancet Diabetes Endocrinol*. Feb 2025;13(2):134-148. [doi: [10.1016/S2213-8587\(24\)00318-8](https://doi.org/10.1016/S2213-8587(24)00318-8)] [Medline: [39681121](#)]

17. Soldera J, Corso LL, Rech MM, et al. Predicting major adverse cardiovascular events after orthotopic liver transplantation using a supervised machine learning model: a cohort study. *World J Hepatol*. Feb 27, 2024;16(2):193-210. [doi: [10.4254/wjh.v16.i2.193](https://doi.org/10.4254/wjh.v16.i2.193)] [Medline: [38495288](#)]

18. Meng D, Zhang L, Cao G, Cao W, Zhang G, Hu B. Liver fibrosis classification based on transfer learning and FCNet for ultrasound images. *IEEE Access*. 2017;5:1-1. [doi: [10.1109/ACCESS.2017.2689058](https://doi.org/10.1109/ACCESS.2017.2689058)]

19. Wang Z, Bian H, Li J, et al. Detection and subtyping of hepatic echinococcosis from plain CT images with deep learning: a retrospective, multicentre study. *Lancet Digit Health*. Nov 2023;5(11):e754-e762. [doi: [10.1016/S2589-7500\(23\)00136-X](https://doi.org/10.1016/S2589-7500(23)00136-X)] [Medline: [37770335](#)]

20. Xiao W, Huang X, Wang JH, et al. Screening and identifying hepatobiliary diseases through deep learning using ocular images: a prospective, multicentre study. *Lancet Digit Health*. Feb 2021;3(2):e88-e97. [doi: [10.1016/S2589-7500\(20\)30288-0](https://doi.org/10.1016/S2589-7500(20)30288-0)] [Medline: [33509389](#)]

21. Calderaro J, Ghaffari Laleh N, Zeng Q, et al. Deep learning-based phenotyping reclassifies combined hepatocellular-cholangiocarcinoma. *Nat Commun*. Dec 14, 2023;14(1):8290. [doi: [10.1038/s41467-023-43749-3](https://doi.org/10.1038/s41467-023-43749-3)] [Medline: [38092727](#)]

22. Yang Y, Liu J, Sun C, et al. Nonalcoholic fatty liver disease (NAFLD) detection and deep learning in a Chinese community-based population. *Eur Radiol*. Aug 2023;33(8):5894-5906. [doi: [10.1007/s00330-023-09515-1](https://doi.org/10.1007/s00330-023-09515-1)] [Medline: [36892645](#)]

23. Wang K, Cunha GM, Hasenstab K, et al. Deep learning for inference of hepatic proton density fat fraction from T1-weighted in-phase and opposed-phase MRI: retrospective analysis of population-based trial data. *AJR Am J Roentgenol*. Nov 2023;221(5):620-631. [doi: [10.2214/AJR.23.29607](https://doi.org/10.2214/AJR.23.29607)] [Medline: [37466189](#)]

24. Zhou LQ, Wang JY, Yu SY, et al. Artificial intelligence in medical imaging of the liver. *World J Gastroenterol*. Feb 14, 2019;25(6):672-682. [doi: [10.3748/wjg.v25.i6.672](https://doi.org/10.3748/wjg.v25.i6.672)] [Medline: [30783371](#)]

25. Reitsma JB, Glas AS, Rutjes AWS, Scholten R, Bossuyt PM, Zwinderman AH. Bivariate analysis of sensitivity and specificity produces informative summary measures in diagnostic reviews. *J Clin Epidemiol*. Oct 2005;58(10):982-990. [doi: [10.1016/j.jclinepi.2005.02.022](https://doi.org/10.1016/j.jclinepi.2005.02.022)] [Medline: [16168343](#)]

26. Cohen JF, Deeks JJ, Hooft L, et al. Preferred reporting items for journal and conference abstracts of systematic reviews and meta-analyses of diagnostic test accuracy studies (PRISMA-DTA for Abstracts): checklist, explanation, and elaboration. *BMJ*. Mar 15, 2021;372:n265. [doi: [10.1136/bmj.n265](https://doi.org/10.1136/bmj.n265)] [Medline: [33722791](#)]

27. Whiting PF, Rutjes AWS, Westwood ME, et al. QUADAS-2: a revised tool for the quality assessment of diagnostic accuracy studies. *Ann Intern Med*. Oct 18, 2011;155(8):529-536. [doi: [10.7326/0003-4819-155-8-201110180-00009](https://doi.org/10.7326/0003-4819-155-8-201110180-00009)] [Medline: [22007046](#)]

28. Yang R, Zhou Y, Liu W, Shang H. Study on the grading model of hepatic steatosis based on improved DenseNet. *J Healthc Eng*. 2022;2022:9601470. [doi: [10.1155/2022/9601470](https://doi.org/10.1155/2022/9601470)] [Medline: [35340251](#)]

29. Acharya UR, Fujita H, Bhat S, et al. Decision support system for fatty liver disease using GIST descriptors extracted from ultrasound images. *Inf Fusion*. May 2016;29:32-39. [doi: [10.1016/j.inffus.2015.09.006](https://doi.org/10.1016/j.inffus.2015.09.006)]

30. Jeon SK, Lee JM, Joo I, Yoon JH, Lee G. Two-dimensional convolutional neural network using quantitative US for noninvasive assessment of hepatic steatosis in NAFLD. *Radiology*. Apr 2023;307(1):e221510. [doi: [10.1148/radiol.221510](https://doi.org/10.1148/radiol.221510)] [Medline: [36594835](#)]

31. Neogi N, Adhikari A, Roy M. Use of a novel set of features based on texture anisotropy for identification of liver steatosis from ultrasound images: a simple method. *Multimed Tools Appl*. May 2019;78(9):11105-11127. [doi: [10.1007/s11042-018-6675-0](https://doi.org/10.1007/s11042-018-6675-0)]

32. Chen JR, Chao YP, Tsai YW, et al. Clinical value of information entropy compared with deep learning for ultrasound grading of hepatic steatosis. *Entropy (Basel)*. Sep 9, 2020;22(9):1006. [doi: [10.3390/e22091006](https://doi.org/10.3390/e22091006)] [Medline: [33286775](#)]

33. Dubois M, Ronot M, Houssel-Debry P, et al. Performance of B-mode ratio and 2D shear wave elastography for the detection and quantification of hepatic steatosis and fibrosis after liver transplantation. *Eur J Gastroenterol Hepatol*. Feb 2020;32(2):222-230. [doi: [10.1097/MEG.0000000000001500](https://doi.org/10.1097/MEG.0000000000001500)] [Medline: [31464783](#)]

34. Shi X, Ye W, Liu F, et al. Ultrasonic liver steatosis quantification by a learning-based acoustic model from a novel shear wave sequence. *Biomed Eng Online*. Dec 21, 2019;18(1):121. [doi: [10.1186/s12938-019-0742-2](https://doi.org/10.1186/s12938-019-0742-2)] [Medline: [31864367](#)]

35. Jesper D, Klett D, Schellhaas B, et al. Ultrasound-based attenuation imaging for the non-invasive quantification of liver fat - a pilot study on feasibility and inter-observer variability. *IEEE J Transl Eng Health Med*. 2020;8:1800409. [doi: [10.1109/JTEHM.2020.3001488](https://doi.org/10.1109/JTEHM.2020.3001488)] [Medline: [32617199](#)]

36. McHenry S, Park Y, Browning JD, Sayuk G, Davidson NO. Dallas steatosis index identifies patients with nonalcoholic fatty liver disease. *Clin Gastroenterol Hepatol*. Aug 2020;18(9):2073-2080. [doi: [10.1016/j.cgh.2020.01.020](https://doi.org/10.1016/j.cgh.2020.01.020)] [Medline: [31982611](#)]

37. Roy M, Wang F, Vo H, et al. Deep-learning-based accurate hepatic steatosis quantification for histological assessment of liver biopsies. *Lab Invest*. Oct 2020;100(10):1367-1383. [doi: [10.1038/s41374-020-0463-y](https://doi.org/10.1038/s41374-020-0463-y)] [Medline: [32661341](#)]

38. Sun L, Marsh JN, Matlock MK, et al. Deep learning quantification of percent steatosis in donor liver biopsy frozen sections. *EBioMedicine*. Oct 2020;60:103029. [doi: [10.1016/j.ebiom.2020.103029](https://doi.org/10.1016/j.ebiom.2020.103029)] [Medline: [32980688](#)]

39. Chou TH, Yeh HJ, Chang CC, et al. Deep learning for abdominal ultrasound: a computer-aided diagnostic system for the severity of fatty liver. *J Chin Med Assoc*. Sep 1, 2021;84(9):842-850. [doi: [10.1097/JCMA.0000000000000585](https://doi.org/10.1097/JCMA.0000000000000585)] [Medline: [34282076](#)]

40. Constantinescu EC, Udrîștoiu AL, Udrîștoiu Stefan C, et al. Transfer learning with pre-trained deep convolutional neural networks for the automatic assessment of liver steatosis in ultrasound images. *Med Ultrason*. May 20, 2021;23(2):135-139. [doi: [10.11152/mu-2746](https://doi.org/10.11152/mu-2746)] [Medline: [33626114](#)]

41. Pérez-Sanz F, Riquelme-Pérez M, Martínez-Barba E, et al. Efficiency of machine learning algorithms for the determination of macrovesicular steatosis in frozen sections stained with Sudan to evaluate the quality of the graft in liver transplantation. *Sensors (Basel)*. Mar 12, 2021;21(6):1993. [doi: [10.3390/s21061993](https://doi.org/10.3390/s21061993)] [Medline: [33808978](#)]

42. Pickhardt PJ, Blake GM, Graffy PM, et al. Liver steatosis categorization on contrast-enhanced CT using a fully automated deep learning volumetric segmentation tool: evaluation in 1204 healthy adults using unenhanced CT as a reference standard. *AJR Am J Roentgenol*. Aug 2021;217(2):359-367. [doi: [10.2214/AJR.20.24415](https://doi.org/10.2214/AJR.20.24415)] [Medline: [32936018](#)]

43. Rhyou SY, Yoo JC. Cascaded deep learning neural network for automated liver steatosis diagnosis using ultrasound images. *Sensors (Basel)*. Aug 5, 2021;21(16):16. [doi: [10.3390/s21165304](https://doi.org/10.3390/s21165304)] [Medline: [34450746](#)]

44. Destrempe F, Gesnik M, Chayer B, et al. Quantitative ultrasound, elastography, and machine learning for assessment of steatosis, inflammation, and fibrosis in chronic liver disease. *PLoS One*. 2022;17(1):e0262291. [doi: [10.1371/journal.pone.0262291](https://doi.org/10.1371/journal.pone.0262291)] [Medline: [35085294](#)]

45. Alshagathrh FM, Musleh S, Alzubaidi M, Schneider J, Househ MS. Efficient detection of hepatic steatosis in ultrasound images using convolutional neural networks: a comparative study. *Trait du Signa*. Oct 30, 2023;40(5):1781-1794. [doi: [10.18280/ts.400501](https://doi.org/10.18280/ts.400501)]

46. Podder S, Mallick A, Das S, Sau K, Roy A. Accurate diagnosis of liver diseases through the application of deep convolutional neural network on biopsy images. 2023;10(4):453-481. [doi: [10.3934/biophy.2023026](https://doi.org/10.3934/biophy.2023026)]

47. Ibrahim MN, Blázquez-García R, Lightstone A, et al. Automated fatty liver disease detection in point-of-care ultrasound b-mode images. *J Med Imaging (Bellingham)*. May 2023;10(3):034505. [doi: [10.1117/1.JMI.10.3.034505](https://doi.org/10.1117/1.JMI.10.3.034505)] [Medline: [37284231](#)]

48. Yao Y, Zhang Z, Peng B, Tang J. Bio-inspired network for diagnosing liver steatosis in ultrasound images. *Bioengineering (Basel)*. Jun 26, 2023;10(7):768. [doi: [10.3390/bioengineering10070768](https://doi.org/10.3390/bioengineering10070768)] [Medline: [37508795](#)]

49. Byra M, Styczynski G, Szmigielski C, et al. Transfer learning with deep convolutional neural network for liver steatosis assessment in ultrasound images. *Int J Comput Assist Radiol Surg*. Dec 2018;13(12):1895-1903. [doi: [10.1007/s11548-018-1843-2](https://doi.org/10.1007/s11548-018-1843-2)] [Medline: [30094778](#)]

50. Torgersen J, Akers S, Huo Y, et al. Performance of an automated deep learning algorithm to identify hepatic steatosis within noncontrast computed tomography scans among people with and without HIV. *Pharmacoepidemiol Drug Saf*. Oct 2023;32(10):1121-1130. [doi: [10.1002/pds.5648](https://doi.org/10.1002/pds.5648)] [Medline: [37276449](#)]

51. Wang Q, Lai MW, Bin G, et al. MBR-Net: a multi-branch residual network based on ultrasound backscattered signals for characterizing pediatric hepatic steatosis. *Ultrasonics*. Dec 2023;135:107093. [doi: [10.1016/j.ultras.2023.107093](https://doi.org/10.1016/j.ultras.2023.107093)] [Medline: [37482038](#)]

52. Jeon SK, Joo I, Park J, Yoo J. Automated hepatic steatosis assessment on dual-energy CT-derived virtual non-contrast images through fully-automated 3D organ segmentation. *Radiol Med*. Jul 2024;129(7):967-976. [doi: [10.1007/s11547-024-01833-8](https://doi.org/10.1007/s11547-024-01833-8)] [Medline: [38869829](#)]

53. Piella G, Farré N, Esono D, et al. LiverColor: an artificial intelligence platform for liver graft assessment. *Diagnostics (Basel)*. Jul 31, 2024;14(15):15. [doi: [10.3390/diagnostics14151654](https://doi.org/10.3390/diagnostics14151654)] [Medline: [39125531](#)]

54. Yoo J, Joo I, Jeon SK, Park J, Yoon SH. Utilizing fully-automated 3D organ segmentation for hepatic steatosis assessment with CT attenuation-based parameters. *Eur Radiol*. Sep 2024;34(9):6205-6213. [doi: [10.1007/s00330-024-10660-4](https://doi.org/10.1007/s00330-024-10660-4)] [Medline: [38393403](#)]

55. Zhang Z, Li G, Wang Z, et al. Deep-learning segmentation to select liver parenchyma for categorizing hepatic steatosis on multinational chest CT. *Sci Rep*. 2024;14(1):11987. [doi: [10.1038/s41598-024-62887-2](https://doi.org/10.1038/s41598-024-62887-2)]

56. Cherchi V, Mea VD, Terrosu G, et al. Assessment of hepatic steatosis based on needle biopsy images from deceased donor livers. *Clin Transplant*. Mar 2022;36(3):e14557. [doi: [10.1111/ctr.14557](https://doi.org/10.1111/ctr.14557)] [Medline: [34890087](#)]

57. Wu X, Lv K, Wu S, Tai DI, Tsui PH, Zhou Z. Parallelized ultrasound homodyned-K imaging based on a generalized artificial neural network estimator. *Ultrasonics*. Jul 2023;132:106987. [doi: [10.1016/j.ultras.2023.106987](https://doi.org/10.1016/j.ultras.2023.106987)] [Medline: [36958066](#)]

58. Drazinos P, Gatos I, Katsakiori PF, et al. Comparison of deep learning schemes in grading non-alcoholic fatty liver disease using b-mode ultrasound hepatorenal window images with liver biopsy as the gold standard. *Phys Med*. Jan 2025;129:104862. [doi: [10.1016/j.ejmp.2024.104862](https://doi.org/10.1016/j.ejmp.2024.104862)] [Medline: [39626614](#)]

59. Kaffas AE, Bhatraju KC, Vo-Phamhi JM, et al. Development of a deep learning model for classification of hepatic steatosis from clinical standard ultrasound. *Ultrasound Med Biol*. Feb 2025;51(2):242-249. [doi: [10.1016/j.ultrasmedbio.2024.09.020](https://doi.org/10.1016/j.ultrasmedbio.2024.09.020)] [Medline: [39537545](#)]

60. Kim HY, Lee KJ, Lee SS, et al. Diagnosis of moderate-to-severe hepatic steatosis using deep learning-based automated attenuation measurements on contrast-enhanced CT. *Abdom Radiol (NY)*. Sep 2025;50(9):4139-4147. [doi: [10.1007/s00261-025-04872-5](https://doi.org/10.1007/s00261-025-04872-5)] [Medline: [40095018](#)]

61. Zhang H, Liu J, Su D, et al. Diagnostic of fatty liver using radiomics and deep learning models on non-contrast abdominal CT. *PLoS ONE*. 2025;20(2):e0310938. [doi: [10.1371/journal.pone.0310938](https://doi.org/10.1371/journal.pone.0310938)] [Medline: [39946425](#)]

62. Derstine BA, Holcombe SA, Chen VL, et al. Quantification of hepatic steatosis on post-contrast computed tomography scans using artificial intelligence tools. *Abdom Radiol*. 2025. [doi: [10.1007/s00261-025-05137-x](https://doi.org/10.1007/s00261-025-05137-x)]

63. Del Corso G, Pascali MA, Caudai C, et al. ANN uncertainty estimates in assessing fatty liver content from ultrasound data. *Comput Struct Biotechnol J*. Dec 2024;24:603-610. [doi: [10.1016/j.csbj.2024.09.021](https://doi.org/10.1016/j.csbj.2024.09.021)] [Medline: [39421530](#)]

64. Hernaez R, Lazo M, Bonekamp S, et al. Diagnostic accuracy and reliability of ultrasonography for the detection of fatty liver: a meta-analysis. *Hepatology*. Sep 2, 2011;54(3):1082-1090. [doi: [10.1002/hep.24452](https://doi.org/10.1002/hep.24452)] [Medline: [21618575](#)]

65. Park HJ, Kim KW, Kwon HJ, et al. CT-based visual grading system for assessment of hepatic steatosis: diagnostic performance and interobserver agreement. *Hepatol Int*. Oct 2022;16(5):1075-1084. [doi: [10.1007/s12072-022-10373-0](https://doi.org/10.1007/s12072-022-10373-0)] [Medline: [35789473](https://pubmed.ncbi.nlm.nih.gov/35789473/)]
66. Azizi N, Naghibi H, Shakiba M, et al. Evaluation of MRI proton density fat fraction in hepatic steatosis: a systematic review and meta-analysis. *Eur Radiol*. Apr 2025;35(4):1794-1807. [doi: [10.1007/s00330-024-11001-1](https://doi.org/10.1007/s00330-024-11001-1)] [Medline: [39254718](https://pubmed.ncbi.nlm.nih.gov/39254718/)]
67. Tapper EB, Lok ASF. Use of liver imaging and biopsy in clinical practice. *N Engl J Med*. Aug 24, 2017;377(8):756-768. [doi: [10.1056/NEJMra1610570](https://doi.org/10.1056/NEJMra1610570)] [Medline: [28834467](https://pubmed.ncbi.nlm.nih.gov/28834467/)]
68. Petroff D, Blank V, Newsome PN, et al. Assessment of hepatic steatosis by controlled attenuation parameter using the M and XL probes: an individual patient data meta-analysis. *Lancet Gastroenterol Hepatol*. Mar 2021;6(3):185-198. [doi: [10.1016/S2468-1253\(20\)30357-5](https://doi.org/10.1016/S2468-1253(20)30357-5)] [Medline: [33460567](https://pubmed.ncbi.nlm.nih.gov/33460567/)]
69. Siddiqui MS, Vuppulanchi R, Van Natta ML, et al. Vibration-controlled transient elastography to assess fibrosis and steatosis in patients with nonalcoholic fatty liver disease. *Clin Gastroenterol Hepatol*. Jan 2019;17(1):156-163. [doi: [10.1016/j.cgh.2018.04.043](https://doi.org/10.1016/j.cgh.2018.04.043)] [Medline: [29705261](https://pubmed.ncbi.nlm.nih.gov/29705261/)]
70. Hepburn MJ, Vos JA, Fillman EP, Lawitz EJ. The accuracy of the report of hepatic steatosis on ultrasonography in patients infected with hepatitis C in a clinical setting: a retrospective observational study. *BMC Gastroenterol*. Apr 13, 2005;5:14. [doi: [10.1186/1471-230X-5-14](https://doi.org/10.1186/1471-230X-5-14)] [Medline: [15829009](https://pubmed.ncbi.nlm.nih.gov/15829009/)]
71. Fischer MA, Reiner CS, Raptis D, et al. Quantification of liver iron content with CT-added value of dual-energy. *Eur Radiol*. Aug 2011;21(8):1727-1732. [doi: [10.1007/s00330-011-2119-1](https://doi.org/10.1007/s00330-011-2119-1)] [Medline: [21472472](https://pubmed.ncbi.nlm.nih.gov/21472472/)]
72. Loizillon S, Bottani S, Maire A, et al. Automatic quality control of brain 3D FLAIR MRIs for a clinical data warehouse. *Med Image Anal*. Jul 2025;103:103617. [doi: [10.1016/j.media.2025.103617](https://doi.org/10.1016/j.media.2025.103617)] [Medline: [40344945](https://pubmed.ncbi.nlm.nih.gov/40344945/)]
73. Ma J, He Y, Li F, Han L, You C, Wang B. Segment anything in medical images. *Nat Commun*. Jan 22, 2024;15(1):654. [doi: [10.1038/s41467-024-44824-z](https://doi.org/10.1038/s41467-024-44824-z)] [Medline: [38253604](https://pubmed.ncbi.nlm.nih.gov/38253604/)]
74. Sheller MJ, Edwards B, Reina GA, et al. Federated learning in medicine: facilitating multi-institutional collaborations without sharing patient data. *Sci Rep*. Jul 28, 2020;10(1):12598. [doi: [10.1038/s41598-020-69250-1](https://doi.org/10.1038/s41598-020-69250-1)] [Medline: [32724046](https://pubmed.ncbi.nlm.nih.gov/32724046/)]
75. Vianna P, Calce SI, Boustros P, et al. Comparison of radiologists and deep learning for US grading of hepatic steatosis. *Radiology*. Oct 2023;309(1):e230659. [doi: [10.1148/radiol.230659](https://doi.org/10.1148/radiol.230659)] [Medline: [37787678](https://pubmed.ncbi.nlm.nih.gov/37787678/)]
76. Zögeler T, Kavallar AM, Pollio AR, et al. Meta-analysis of shotgun sequencing of gut microbiota in obese children with MASLD or MASH. *Gut Microbes*. Dec 2025;17(1):2508951. [doi: [10.1080/19490976.2025.2508951](https://doi.org/10.1080/19490976.2025.2508951)] [Medline: [40396204](https://pubmed.ncbi.nlm.nih.gov/40396204/)]
77. Hou M, Zhu Y, Zhou H, et al. Innovative machine learning approach for liver fibrosis and disease severity evaluation in MAFLD patients using MRI fat content analysis. *Clin Exp Med*. Aug 5, 2025;25(1):275. [doi: [10.1007/s10238-025-01818-5](https://doi.org/10.1007/s10238-025-01818-5)] [Medline: [40762814](https://pubmed.ncbi.nlm.nih.gov/40762814/)]
78. Wei Y, Yang M, Zhang M, et al. Focal liver lesion diagnosis with deep learning and multistage CT imaging. *Nat Commun*. 2024;15(1):7040. [doi: [10.1038/s41467-024-51260-6](https://doi.org/10.1038/s41467-024-51260-6)] [Medline: [39147767](https://pubmed.ncbi.nlm.nih.gov/39147767/)]
79. Dunn N, Verma N, Dunn W. Artificial Intelligence for predictive diagnostics, prognosis, and decision support in MASLD, hepatocellular carcinoma, and digital pathology. *J Clin Exp Hepatol*. 2026;16(1):103184. [doi: [10.1016/j.jceh.2025.103184](https://doi.org/10.1016/j.jceh.2025.103184)] [Medline: [41127419](https://pubmed.ncbi.nlm.nih.gov/41127419/)]
80. Raji CG, Chandra SSV, Gracious N, Pillai YR, Sasidharan A. Advanced prognostic modeling with deep learning: assessing long-term outcomes in liver transplant recipients from deceased and living donors. *J Transl Med*. Feb 16, 2025;23(1):188. [doi: [10.1186/s12967-025-06183-1](https://doi.org/10.1186/s12967-025-06183-1)] [Medline: [39956905](https://pubmed.ncbi.nlm.nih.gov/39956905/)]
81. Guillot J, Williams CYK, Azzam S, et al. Risk prediction in patients with metabolic dysfunction-associated steatohepatitis using natural language processing. *Gastro Hep Adv*. 2025;4(9):100701. [doi: [10.1016/j.gastha.2025.100701](https://doi.org/10.1016/j.gastha.2025.100701)] [Medline: [40688387](https://pubmed.ncbi.nlm.nih.gov/40688387/)]
82. Zhang J, Feng S, Xue J, et al. AI-driven multimodal fusion of tongue images and clinical indicators for identifying MAFLD patients at risk of coronary artery disease: an exploratory study. *ILIVER*. Sep 2025;4(3):100181. [doi: [10.1016/j.iliver.2025.100181](https://doi.org/10.1016/j.iliver.2025.100181)] [Medline: [41054419](https://pubmed.ncbi.nlm.nih.gov/41054419/)]
83. Li B, Tai DI, Yan K, et al. Accurate and generalizable quantitative scoring of liver steatosis from ultrasound images via scalable deep learning. *World J Gastroenterol*. Jun 14, 2022;28(22):2494-2508. [doi: [10.3748/wjg.v28.i22.2494](https://doi.org/10.3748/wjg.v28.i22.2494)] [Medline: [35979264](https://pubmed.ncbi.nlm.nih.gov/35979264/)]
84. Determination of signal-to-noise ratio (SNR) in diagnostic magnetic resonance imaging. NEMA; 2021. URL: <https://www.nema.org/Standards/view/Determination-of-Signal-to-Noise-Ratio-in-Diagnostic-Magnetic-Resonance-Imaging> [Accessed 2021-03-31]

85. Lee B, Kramer P, Sandri S, et al. Early recalls and clinical validation gaps in artificial intelligence-enabled medical devices. *JAMA Health Forum*. Aug 1, 2025;6(8):e253172. [doi: [10.1001/jamahealthforum.2025.3172](https://doi.org/10.1001/jamahealthforum.2025.3172)] [Medline: [40844774](https://pubmed.ncbi.nlm.nih.gov/40844774/)]
86. Li YH, Li YL, Wei MY, Li GY. Innovation and challenges of artificial intelligence technology in personalized healthcare. *Sci Rep*. Aug 16, 2024;14(1):18994. [doi: [10.1038/s41598-024-70073-7](https://doi.org/10.1038/s41598-024-70073-7)] [Medline: [39152194](https://pubmed.ncbi.nlm.nih.gov/39152194/)]
87. Bhandari M, Zeffiro T, Reddiboina M. Artificial intelligence and robotic surgery: current perspective and future directions. *Curr Opin Urol*. Jan 2020;30(1):48-54. [doi: [10.1097/MOU.0000000000000692](https://doi.org/10.1097/MOU.0000000000000692)] [Medline: [31724999](https://pubmed.ncbi.nlm.nih.gov/31724999/)]
88. Deshmukh AD, Wagner JK. FDA draft guidelines for AI and the need for ethical frameworks. *JAMA Pediatr*. Sep 1, 2025;179(9):937-938. [doi: [10.1001/jamapediatrics.2025.1979](https://doi.org/10.1001/jamapediatrics.2025.1979)] [Medline: [40622691](https://pubmed.ncbi.nlm.nih.gov/40622691/)]

## Abbreviations

**AI:** artificial intelligence

**AUC:** area under curve

**DL:** deep learning

**HCC:** hepatocellular carcinoma

**HS:** hepatic steatosis

**LRN:** negative likelihood ratio

**LRP:** positive likelihood ratio

**MAFLD:** metabolic dysfunction associated fatty liver disease

**ML:** machine learning

**MRI:** magnetic resonance imaging

**MRI-PDFF:** magnetic resonance imaging-proton density fat fraction

**PRISMA-DTA:** Preferred Reporting Items for Systematic Reviews and Meta-Analyses—Diagnostic Test Accuracy

**PRISMA-S:** Preferred Reporting Items for Systematic Reviews and Meta-Analyses—Search Extension

**SROC:** summary receiver operating characteristic

**TL:** transfer learning

*Edited by Stefano Brini; peer-reviewed by Jonathan Soldera, Kuan-Hsun Lin, Mahmoud Badee Rokaya Mahmoud; submitted 30.May.2025; final revised version received 11.Nov.2025; accepted 11.Nov.2025; published 13.Jan.2026*

*Please cite as:*

*Song J, Liu D, Li J, Cong H, Deng R, Lu Y, Sun J, Zhang J*

*Assessment of the Diagnostic Performance and Clinical Impact of AI in Hepatic Steatosis: Systematic Review and Meta-Analysis*

*J Med Internet Res* 2026;28:e78310

*URL:* <https://www.jmir.org/2026/1/e78310>

*doi:* [10.2196/78310](https://doi.org/10.2196/78310)

© Jiamei Song, Dan Liu, Jitong Li, Haoru Cong, Ruixue Deng, Yihan Lu, Jiayi Sun, Jingzhou Zhang. Originally published in the Journal of Medical Internet Research (<https://www.jmir.org>), 13.Jan.2026. This is an open-access article distributed under the terms of the Creative Commons Attribution License (<https://creativecommons.org/licenses/by/4.0/>), which permits unrestricted use, distribution, and reproduction in any medium, provided the original work, first published in the Journal of Medical Internet Research (ISSN 1438-8871), is properly cited. The complete bibliographic information, a link to the original publication on <https://www.jmir.org/>, as well as this copyright and license information must be included.